crystals

MDPI

Review

Transition Metal Selenite Halides: A Fascinating Family of Magnetic Compounds

Peter S. Berdonosov *, Elena S. Kuznetsova and Valery A. Dolgikh

Department of Chemistry of Lomonosov Moscow State University, Moscow 119991, Russia; e.kuznetsova@inorg.chem.msu.ru (E.S.K.); dolgikh@inorg.chem.msu.ru (V.A.D.)

* Correspondence: berdonosov@inorg.chem.msu.ru; Tel.: +7-495-939-3504

Received: 12 March 2018; Accepted: 2 April 2018; Published: 4 April 2018

Abstract: The problem of searching for low-dimensional magnetic systems has been a topical subject and has attracted attention of the chemistry and physics community for the last decade. In low-dimensional magnetic systems, magnetic ions are distributed anisotopically and form different groups such as dimers, chains, ladders, or planes. In 3D frameworks, the distances between magnetic ions are equal in all directions while in low-dimensional systems the distances within groups are different from those between groups. The main approach of searching for desired systems is a priori crystal chemical design expecting the needed distribution of transition metal ions in the resulting structure. One of the main concepts of this structural design is the incorporation of the *p*-element ions with stereochemically active electron pairs and ions acting as spacers in the composition. Transition metal selenite halides, substances that combine SeO_3^{2-} groups and halide ions in the structure, seem to be a promising object of investigation. Up to now, there are 33 compounds that are structurally described, magnetically characterized, and empirically tested on different levels. The presented review will summarize structural peculiarities and observed magnetic properties of the known transition metal selenite halides. In addition, the known compounds will be analyzed as possible low-dimensional magnetic systems.

Keywords: selenite; selenite halide; crystal structure; transition metal; magnetic structure

1. Introduction

In recent decades, approaches for the search for and synthesis of low-dimensional magnets, that is, the systems with magnetic ions distributed anisotropically in the crystal structure and forming different types of groups as dimers, trimers, tetramers or isolated plaquette units, chains of ions, ladders, or planes, have been attracting considerable interest from the physics and chemistry research communities. Such geometric distribution of magnetic ions may lead to exotic magnetic states such as spin liquids or geometric magnetic spin frustrations which are hot topics in the physics of condensed matter [1,2]. In the usual three-dimensional structures, the magnetic exchange between magnetic ions is equal in all directions whereas in low-dimensional systems the exchange within the above-mentioned groups is much stronger than between the groups.

The interest in low-dimensional magnetic systems has resulted, on the one hand, from their fundamental importance as model objects for the verification of theoretical predictions in condensed matter physics theory and on the other hand, from their possible applications, for example, for tunable heat conduction discussed in [3]. Until now, the compounds studied from this point of view in inorganic chemistry are usually limited to oxide systems, chalcogenide compounds, and sometimes halides [2]. Currently, one of the main avenues for the search for low-dimensional magnetic compounds is the targeted synthesis of new compounds using the a priori structure design suggesting a special distribution of magnetic transition metal ions in the final crystal structure. It should be kept in mind

that a structural sublattice of ions could be different from the real magnetic exchange path but the probability to find a low-dimensional magnetic sublattice in a low-dimensional crystal structure should be higher. The structural influence of stereochemically active electron pairs of *p*-elements in the middle oxidation states, such as Bi(III), Pb(II), Te(IV), Se(IV) etc. appears to be an unattractive synthesis concept in the search for low-dimensional magnetic systems. A lone electron pair is non-bonding and plays a role of the additional ligand for the central ion. According to the Valence Shell Electron Pair Repulsion theory [4,5] such ions in the oxidation state +4 should have a stereochemically active electron pair which distorts the selenium environment. As a result, one side of the ion is not bonded to other atoms in the crystal structure and electron pairs form cavities or holes in the crystal structure. According to [6], the volume of the non-bonding pair of electrons is compatible to that of the O^{2-} ion. Sometimes [7] ions with electron pairs are referred to as 'chemical scissors' which are "cutting through" the 3D crystal structure. The resulting structure cavity may be extended even to a layer by introducing the additional terminating ions (spacers), for example, halide ions.

By now, many transition metal selenite halides have been synthesized and characterized. The majority of these compounds contain copper in the oxidation state +2. Some compounds in the mentioned group have been characterized magnetically by different techniques. In accordance with the above-mentioned concept, it appears useful to summarize the information about the known compounds including their crystal structures and magnetic characterization, which will be the subject of the present review.

Usually the selenite group SeO_3^{2-} possesses a pyramidal shape (C_{3v} symmetry in the free state) with distances Se–O are about 1.73 Å and O–Se–O angles are 103° [8]. In addition, the SeO_3^{2-} group may be described as a pseudo-tetrahedral anion with the lone electron pair acting as an invisible ligand in the crystal structures. The observation of lone electron pairs in selenites is one of their structural peculiarities. In the solid state, the C_{3v} symmetry of SeO_3^{2-} groups is distorted due to the differences in the connectivity. In contrast to sulfur, the +4 oxidation state is more stable for selenium due to the small value of redox potential SeO_4^{2-}/SeO_3^{2-} 0.05 V which is positive in alkaline solutions whereas the corresponding value for SO_4^{2-}/SO_3^{2-} is much lower −0.93 V. This makes selenites more stable in solutions compared to sulfites [8,9]. Tellurium has a larger radius and may form not only TeO_3^{2-} tellurite groups but display higher coordination numbers, 3 + 1 for example. Moreover, tellurites often tend to form polyions with different compositions and geometry [7,10].

Combining the transition ions, selenite, or tellurite groups with halide ions within one structure may lead to the novel crystal structures and different magnetic properties [11–15]. It is easy to note that up to now transition metal tellurite halide compounds are more explored. There are two factors which account for this. First one is the oxidizing activity of selenites. In water solution, the reduction potential SeO_3^{2-}/Se is −0.336 V [9]. For this reason, it will be difficult to combine Ti^{3+}, V^{3+} ions with selenites, while tellurites tend to be more stable. Another reason for tellurites being more studied is the stability of tellurium dioxide in the air and consequently its facile synthetic preparation. Selenium dioxide is air- and moisture-sensitive, hence all preparative procedures with it are usually performed under dry conditions (i.e., argon or nitrogen filled glove boxes), in order to avoid the formation of hydrates or hydroselenites. As it will be shown below, chlorides are the most representative group among halides, whereas iodides were obtained in one case only. The reason for this seems to be lying in the oxidizing effect of the selenite groups.

Usually, transition metal ions are responsible for the magnetic behavior of substances. From this point of view, 3d metals in middle oxidation states are most attractive as 4d and 5d metals in low oxidation states may bind together and the magnetic moment of metal ions disappears [16]. The literature search shows that up to now there are no data about crystal structures and magnetic properties of 4d and 5d transition metal selenite halides (taking into account that compound $Pb_2NbO_2(SeO_3)_2Cl$ [17] contains Nb in the oxidation state +5 and d^0 configuration). Therefore, in this review we will describe crystal structures and some reported magnetic properties of 3d metal selenite halides, that is, compounds containing both SeO_3^{2-} groups and halide ions.

2. Crystal Structures and Magnetic Properties Overview

Here we will describe the crystal structures of complex transition metal selenite halides with known magnetic properties. The term "halide ions" will refer to chlorides, bromides, and sometimes iodides. Fluoride compounds usually show different behavior and tendencies due to the peculiarities of fluorine and fluorides sometimes are closer to pure oxide compounds. Moreover, the literature data about selenite fluorides or oxofluorides of d-metals are rather limited and describe only a small number of compounds [18–21].

Below, we will pay special attention to the transition metal M–M ions distances in the structures. It should be noted, that this is an oversimplified way of considering the spin interactions. For a precise estimation, the geometry of d-orbitals and their interactions with the orbitals of bridged atoms should be examined. Nevertheless, it seems that presented simple model may be used at least for crystal chemical design of 3d-metal selenite halide compounds, as in the case of very long M–M distances the probability of spin interactions exchange should be lower.

2.1. Composition $M^{II}{}_5(SeO_3)_4X_2$

The group of compounds under consideration contains 6 different compositions and exists up to now only for Fe, Co, Ni, and Cu. Compositions and some crystallographic information are given in Table 1. As can be seen from Table 1, the crystal structures for these compounds are different in compositions and cell symmetries.

The substances may be divided into several groups according to their common composition and structural relations.

The first group of transition metal selenite halides may be described by the composition $M^{II}{}_5(SeO_3)_4X_2$ (substances 1–5 in Table 1) [22–25]. While cobalt and nickel compounds are similar in some forms, copper compounds' crystal structures are different. The crystal structure of $Cu_5(SeO_3)_4Cl_2$ is presented in Figure 1 as the projection on *ab* plane.

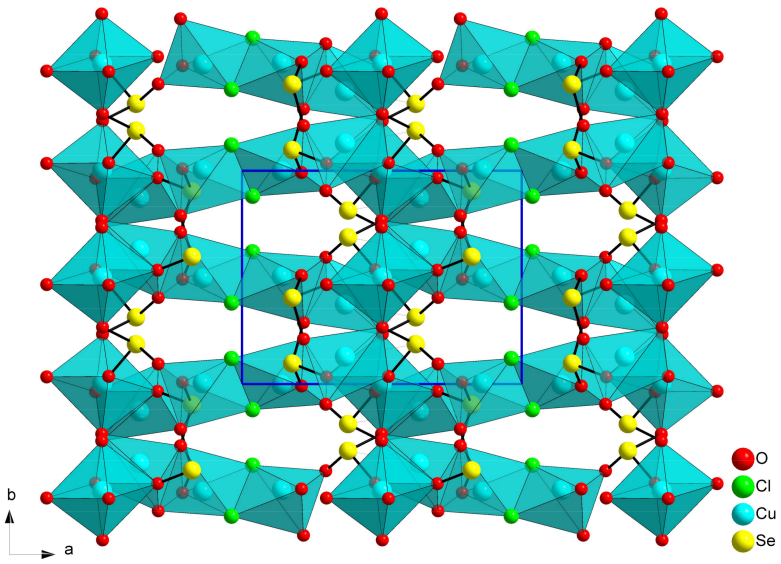

Figure 1. Projection of the $Cu_5(SeO_3)_4Cl_2$ crystal structure on ab plane according to [22]. Copper polyhedra are shown.

The crystal structure of $Cu_5(SeO_3)_4Cl_2$ [20] may be presented as a three-dimensional framework of corner- and edge-shared polyhedra [CuO_5], [CuO_6], and [CuO_3Cl_2]. It is easy to see in Figure 1 that the framework of Cu polyhedra contains wide holes where selenium atoms are located. Due to the pyramidal shape and the presence of the E-pairs in SeO_3^{2-} groups copper polyhedra do not polymerize in more dense packing. According to the structural data, Cu–Cu distances in the crystal

structure of $Cu_5(SeO_3)_4Cl_2$ are in the range of 3.15–3.30 Å and one distance value is about 3.6 Å. One may conclude that spin–spin interactions between Cu^{2+} ions may be observed in this compound.

Field-cooled magnetization measurements data show spontaneous polarization below the critical temperature of $T_C \approx 45$ K. Below this point almost linear magnetization increase and saturation at low temperatures are observed. The heat capacity temperature dependence demonstrates a λ-type anomaly at 44.1(2) K thus confirming magnetization measurements results. The Curie–Weiss temperature calculated from the approximation of experimental data has a value of −151(4) K and indicates predominantly antiferromagnetic spin-exchange interactions. Thus, a long-range antiferromagnetic order occurs in $Cu_5(SeO_3)_4Cl_2$ at 44.1(2) K.

However, field dependent magnetization measurements at 1.87 K reveal a hysteresis loop, indicating the presence of weak ferromagnetic interactions. This is a common phenomenon occurred in complex magnetic systems based on Cu^{2+} ions where low-dimensional magnetic interactions take place. The complexity of exchange paths is due to the numerous distortions of coordination polyhedra in the crystal structure. Analysis of interconnections between copper, chlorine, and oxygen atoms in the $Cu_5(SeO_3)_4Cl_2$ structure revealed two main types of magnetic exchange paths: the first one is the antiferromagnetic path between copper atoms connected via the oxygen atom; the Cu–O–Cu angle value exceeds 90°. The second path is the ferromagnetic path between copper atoms interacting via a chlorine atom. The Cu–Cl–Cu angle is almost 90°—such bonding angles typically support ferromagnetic spin-exchange interactions [22].

Due to the Jahn–Teller effect, the surrounding of Cu^{2+} differs from that of Co^{2+} and Ni^{2+}, and this is the reason for differences between cobalt and nickel compounds and the copper ones. Similar compounds for cobalt and nickel have common structures at least in one form (Table 1, substances 2, 3 and 5 [23,25]). All three metal atoms in the compounds under discussion have a distorted octahedral coordination (Figure 2a). Two atoms have a $[MO_5X]$ (X = Cl and Br) coordination and one M atom has a $[MO_4X_2]$ coordination with the oxygen atoms in the square plane. The O–O edge-sharing $[MO_5X]$ polyhedra form chains which are connected via common halogen vertexes into layers in the crystal structures of cobalt and nickel compounds. A three-dimensional structure appears when such layers are bridged by $[MO_4X_2]$ polyhedrons and SeO_3^{2-} groups (Figure 2a). The crystal structures of $Co_5(SeO_3)_4X_2$ and $Ni_5(SeO_3)_4Br_2$ have M–M distances in the range of 3.10–3.37 Å for $Co_5(SeO_3)_4Cl_2$ [23], 3.07–3.40 Å for $Co_5(SeO_3)_4Br_2$ [23], and 3.03–3.39 Å for $Ni_5(SeO_3)_4Br_2$ [25].

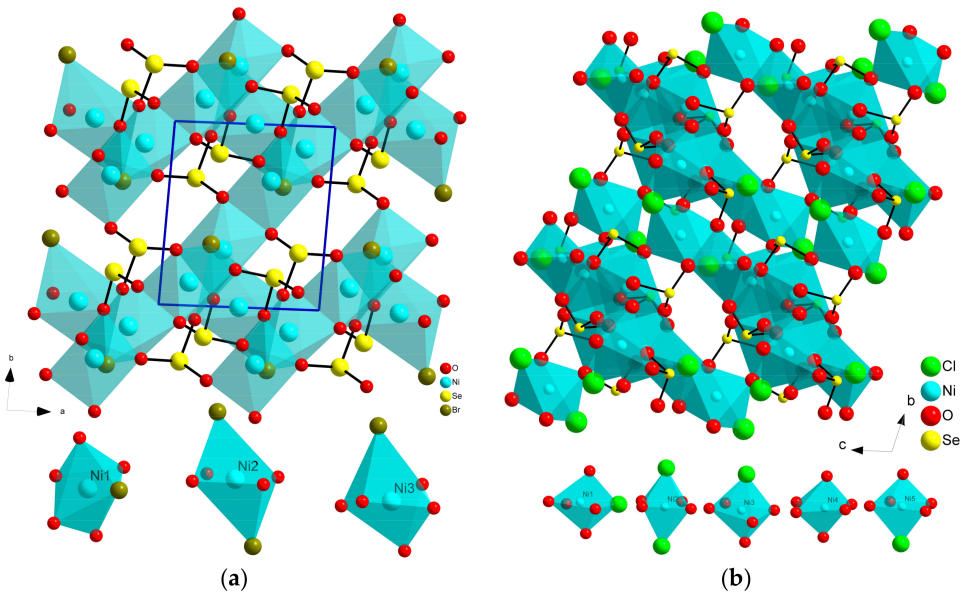

Figure 2. The $Ni_5(SeO_3)_4Br_2$ framework crystal structure (**a**) and $Ni_5(SeO_3)_4Cl_2$ structure (**b**). Coordination surroundings of the Ni atoms are depicted at the bottom part of the pictures.

Table 1. Compositions and crystallographic data for transition metals selenite halides with described magnetic properties.

#	Composition	Space Group	Z	Cell Constants				Ref.
				a, Å	b, Å	c, Å	Angles, °	
1	$Cu_5(SeO_3)_4Cl_2$	$P2_1/c$	2	10.9104(8)	8.3134(6)	7.5490(6)	β = 90.715(6)	[22]
2	$Co_5(SeO_3)_4Cl_2$	P-1	1	6.4935(8)	7.7288(8)	7.7443(10)	α = 66.051(11) β = 73.610(11) γ = 81.268(9)	[23]
3	$Co_5(SeO_3)_4Br_2$	P-1	1	6.4897(9)	7.7574(10)	7.7552(10)	α = 66.850(13) β = 73.960(12) γ = 81.350(11)	[23]
4	$Ni_5(SeO_3)_4Cl_2$	P-1	2	8.076(2)	9.288(2)	9.376(2)	α = 101.97(3) β = 105.60(3) γ = 91.83(3)	[24]
5	$Ni_5(SeO_3)_4Br_2$	P-1	1	6.430(3)	7.632(3)	7.658(3)	α = 68.017(16) β = 74.181(16) γ = 81.465(19)	[25]
6	$Sr_2Co(SeO_3)_2Cl_2$	$P2_1/n$	2	5.3400(10)	6.4279(6)	12.3220(10)	β = 92.440(10)	[26]
7	$Sr_2Ni(SeO_3)_2Cl_2$	$P2_1/n$	2	5.3254(11)	6.4363(13)	12.197(2)	β = 92.53(3)	[26]
8	$Sr_2Cu(SeO_3)_2Cl_2$	$P2_1/n$	2	5.22996(3)	6.50528(4)	12.34518(7)	β = 91.3643(2)	[27]
9	$CaCu_2(SeO_3)_2Cl_2$	C2/c	4	12.759(3)	9.0450(18)	6.9770(14)	β = 91.03(3)	[28]
10	$SrCu_2(SeO_3)_2Cl_2$	$P2_1$	2	7.1630(14)	7.2070(14)	8.0430(16)	β = 95.92(3)	[27]
11	$PbCu_2(SeO_3)_2Cl_2$	C2/c	4	13.056(1)	9.5567(9)	6.9006(6)	β = 90.529(7)	[29]
12	$Bi_2Fe(SeO_3)_2OCl_3$	$P2_1/m$	2	8.570(2)	7.137(2)	8.604(2)	β = 107.090(3)	[30]
13	$Cu_3Bi(SeO_3)_2O_2Cl$	Pmmn	2	6.3540(4)	9.6350(5)	7.2330(4)		[31]
14	$Cu_3Bi(SeO_3)_2O_2Br$	Pmmn	2	6.3900(3)	9.6940(4)	7.2870(3)		[31]
15	$Cu_3Bi(SeO_3)_2O_2I$	Pmmn	2	6.4360(2)	9.7510(4)	7.3770(3)		[31]
16	$Cu_3Y(SeO_3)_2O_2Cl$	Pmmn	2	6.2991(1)	9.4411(1)	6.9724(1)		[32]
17	$Cu_3La(SeO_3)_2O_2Cl$	Pmmn	2	6.39407(18)	9.7310(3)	7.1547(2)		[33]
18	$Cu_3Nd(SeO_3)_2O_2Cl$	Pmmn	2	6.37775(10)	9.62685(16)	7.09341(11)		[31]
19	$Cu_3Sm(SeO_3)_2O_2Cl$	Pmmn	2	6.34616(4)	9.56090(7)	7.04377(5)		[34]
20	$Cu_3Eu(SeO_3)_2O_2Cl$	Pmmn	2	6.3384 (1)	9.5341(2)	7.0273(1)		[35]
21	$Cu_3Gd(SeO_3)_2O_2Cl$	Pmmn	2	6.3220(6)	9.501(1)	7.0202(8		[36]
22	$Cu_3Dy(SeO_3)_2O_2Cl$	Pmmn	2	6.313(1)	9.465(2)	6.987(2)		[36]
23	$Cu_3Ho(SeO_3)_2O_2Cl$	Pmmn	2	6.2999(6)	9.440(1)	6.9723(8)		[36]
24	$Cu_3Er(SeO_3)_2O_2Cl$	Pmmn	2	6.299(1)	9.432(3)	6.967(2)		[36]
25	$Cu_3Yb(SeO_3)_2O_2Cl$	Pmmn	2	6.28278(3)	9.39486(5)	6.93291(3)		[37]
26	$Cu_3Lu(SeO_3)_2O_2Cl$	Pmmn	2	6.2681(1)	9.3756(2)	6.9326(1)		[35]
27	$Cu_3La(SeO_3)_2O_2Br$	Pmmn	2	6.40071(5)	9.75675(7)	7.17800(5)		[33]
28	$Cu_3Nd(SeO_3)_2O_2Br$	Pmmn	2	6.382(2)	9.698(3)	7.091(2)		[36]
29	$Cu_3Sm(SeO_3)_2O_2Br$	Pmmn	2	6.348(1)	9.581(2)	7.079(2)		[36]
30	$Cu_3Gd(SeO_3)_2O_2Br$	Pmmn	2	6.337(1)	9.5515(8)	7.0540(9)		[36]
31	$NaCu_5(SeO_3)_2O_2Cl_3$	Pnma	4	17.769(7)	6.448(3)	10.522(4)		[38]
32	$KCu_5(SeO_3)_2O_2Cl_3$	Pnma	4	18.1691(6)	6.4483(2)	10.5684(4)		[39]
33	$Na_2Cu_7(SeO_3)_4O_2Cl_4$	P-1	1	7.446(2)	8.349(3)	9.137(3)	α = 110.335(7) β = 106.166(3) γ = 105.161(7)	[40]

In spite of the similarity of $Co_5(SeO_3)_4X_2$ (X = Cl and Br) compounds, the nickel chloride is not isostructural with the bromide one [24,41]. The unit cell for $Ni_5(SeO_3)_4Cl_2$ is about twice as

big in volume compared to that of the bromide. There are five Ni atoms in the structure which are octahedrally coordinated by oxygen atoms from SeO_3^{2-} groups or Cl^- ions. There are three types of [NiO_5Cl] and one type of [NiO_4Cl_2] octahedrons and a pure oxygen octahedron [NiO_6] in the structure of $Ni_5(SeO_3)_4Cl_2$ (Figure 2b). Thus, the structure of $Ni_5(SeO_3)_4Cl_2$ features a condensed three-dimensional (3D) network built by Ni^{2+} ions interconnected by SeO_3^{2-} anions as well as Cl^- anions. The crystal structure of $Ni_5(SeO_3)_4Cl_2$ is presented in Figure 2b. It is interesting to mention that Ni–Ni distances in nickel selenite chloride vary from 2.94 up to 3.9 Å [41]. The existence of isostructural compounds for Co with Cl and Br may indicate that $Ni_5(SeO_3)_4Cl_2$ might form two polymorphs. It should be noted that tellurites of the similar composition $Ni_5(TeO_3)_4X_2$ (X = Cl, Br) [12] are isostructural to each other as well as to related cobalt compounds $Co_5(TeO_3)_4X_2$ (X = Cl, Br) [42], but differ from presented selenites. Magnetic properties were studied for $Ni_5(SeO_3)_4Cl_2$ as well as for isostructural compounds $Co_5(SeO_3)_4X_2$ (X = Cl and Br) and $Ni_5(SeO_3)_4Br_2$.

$Ni_5(SeO_3)_4Cl_2$ demonstrates antiferromagnetic properties, according to magnetic susceptibility measurements data. Long-range order takes place at approximately 4.5 K. Curie–Weiss temperature $\theta = -143(2)$ K indicates strong antiferromagnetic interactions between nickel atoms. Such strong interactions take place because of the very short Ni–Ni distances. Moreover, the crystal structure of $Ni_5(SeO_3)_4Cl_2$ is three-dimensional and the network is highly condensed. According to the magnetic measurements data there is no evidence of extraordinary or unusual magnetic behavior in this compound [22], but up to now no detailed study has been undertaken, therefore this problem is still of a certain interest.

Concerning $Co_5(SeO_3)_4X_2$ (X = Cl and Br) and $Ni_5(SeO_3)_4Br_2$, there are also antiferromagnetic transitions in the magnetic subsystems of these compounds (T_N = 18 K, 20 K and 46 K for $Co_5(SeO_3)_4Cl_2$, $Co_5(SeO_3)_4Br_2$, and $Ni_5(SeO_3)_4Br_2$, respectively) [23,25]. However, unlike $Ni_5(SeO_3)_4Cl_2$, magnetic measurements were performed using single crystal samples, and this allowed to carry out a more detailed investigation. In particular, the magnetic susceptibility measurements in oriented crystals revealed anisotropy—typical for the zero-field splitting—induced by the single-ion anisotropy of 3d-metal ions. This allowed defining ground states and electron transitions in these compounds at lower temperatures. Another peculiarity is that the magnetic ordering permeates only one subsystem in the complex magnetic system: a minority fraction is represented in $Co_5(SeO_3)_4X_2$ (X = Cl and Br) ordered subsystem while a magnetically ordered fraction dominates in $Ni_5(SeO_3)_4Br_2$.

2.2. Compositions $Sr_2M^{II}(SeO_3)_2Cl_2$ and $MM''_2(SeO_3)_2Cl_2$

The group of selenites with the composition $Sr_2M^{II}(SeO_3)_2Cl_2$ is presented by isostructural compounds for M^{II} = Co, Ni, and Cu [26,27] (compounds 6–8 in Table 1). The unit cell of these compounds contains one independent atom of Sr and one atom of M. The nearest coordination surrounding of Sr and M atoms comprise oxygen and chlorine atoms, whereas Se atoms have only oxygen atoms as neighbors. In all three compounds, strontium atoms are situated in distorted [SrO_6Cl_3] 9-vertex polyhedra which form layers perpendicular to the [0 0 1] direction of the structure. D-metal ions are allocated in Jahn–Teller distorted octahedrons [MO_4Cl_2]. These polyhedra share common edges with layers of Sr polyhedra and form a 3D structure shown in Figure 3. The M–M distances in the represented structures are longer than 5 Å.

The substitution of one more strontium ion by a d-element ion for compounds $Sr_2M^{II}(SeO_3)_2Cl_2$ is possible for Cu^{2+} and produces $SrCu_2(SeO_3)_2Cl_2$ [27]. This compound is similar to the tellurites $SrCu_2(TeO_3)_2Cl_2$ [43] and $BaCu_2(TeO_3)_2Cl_2$ [44]. These compounds crystallize in the non-centrosymmetrical space group $P2_1$. The crystal structure of $SrCu_2(SeO_3)_2Cl_2$ is given in Figure 4. The asymmetric unit of $SrCu_2(SeO_3)_2Cl_2$ contains one Sr atom and two copper atoms. Sr atom is allocated in the [SrO_6Cl_2] polyhedron and copper atoms are situated in distorted square pyramids [CuO_4Cl] and [CuO_3Cl_2]. It seems that Jahn–Teller distortion in the compound under discussion is much stronger than for a copper atom surrounding in the case of $Sr_2Cu(SeO_3)_2Cl_2$ [27]. Such a strong distortion is impossible for cobalt and nickel and may explain why the same structures are not formed

for them. Both Se atoms in the structure are connected to the strontium or copper polyherda and play the role of an additional linker to form a framework. Copper polyhedra are connected by the common O–Cl edges and form dimers [$Cu_2O_4Cl_2$] (Figure 4). The distance of Cu–Cu in the dimer groups is 3.29 Å which is shorter than 3.35 Å in $SrCu_2(TeO_3)_2Cl_2$ [43].

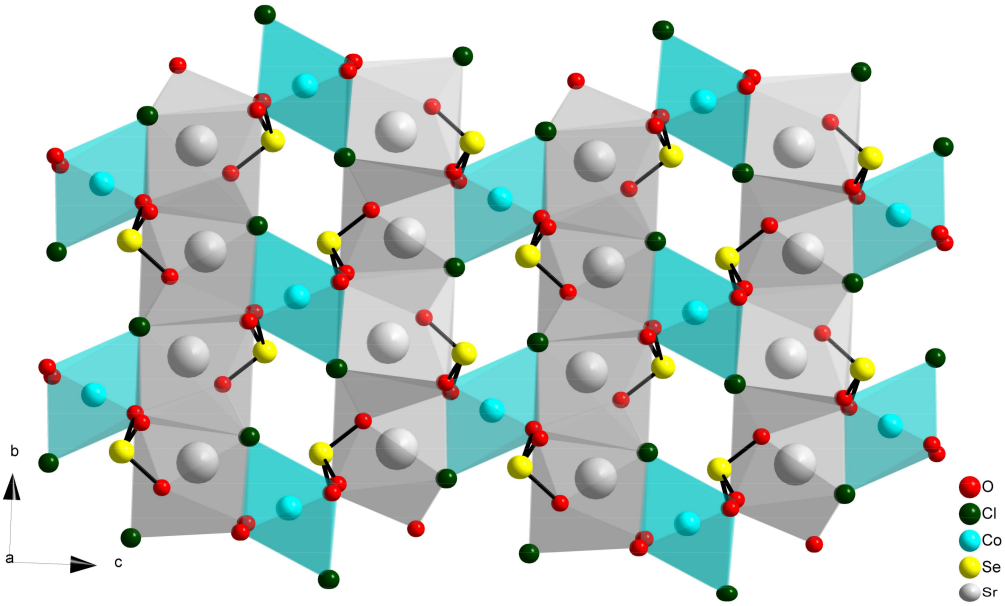

Figure 3. Layers of [SrO_6Cl_3] polyhedral connected by [MO_4Cl_2] octahedra and SeO_3^{2-} groups in the crystal structure of $Sr_2Co(SeO_3)_2Cl_2$ [26].

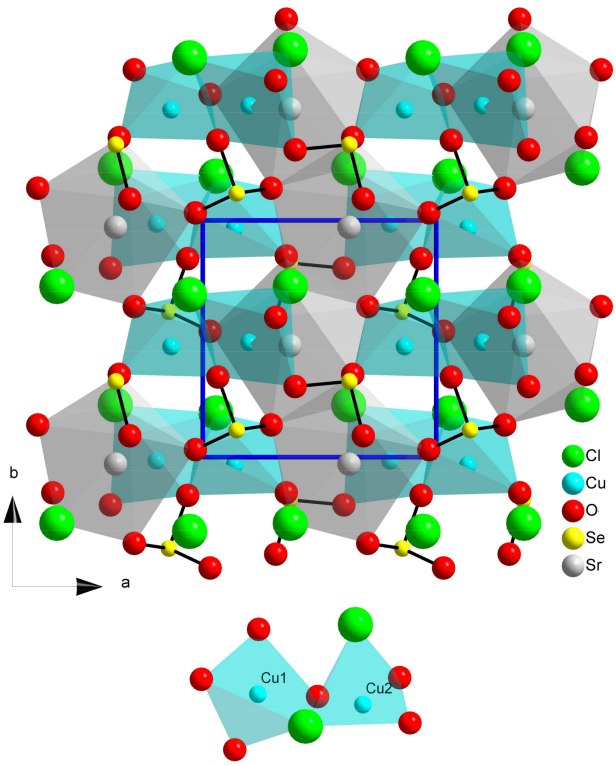

Figure 4. Crystal structure of $SrCu_2(SeO_3)_2Cl_2$ [27]. The [$Cu_2O_4Cl_2$] dimer is shown separately at the bottom part of the figure.

According to Shannon's data [45] the ionic radius of Sr^{2+} ions is close to that of Pb^{2+}. At the same time, according to the Periodic Table of the elements, calcium as an alkali earth metal may be a smaller analog of strontium. There were obtained compounds with compositions $CaCu_2(SeO_3)_2Cl_2$ and $PbCu_2(SeO_3)_2Cl_2$ [28,29] (Table 1 substances 9 and 11). It is apparent (Table 1) that both compounds are isostructural but have a different unit cell in comparison with $SrCu_2(SeO_3)_2Cl_2$ (Table 1 substance 10). At the same time, the tellurite compound $PbCu_2(TeO_3)_2Cl_2$ [29] is isostructural to $SrCu_2(SeO_3)_2Cl_2$ [27]. This phenomenon may be associated with differences in ionic radii of Se^{4+} and Te^{4+}. A bigger tellurium atom is more compatible with strontium or lead, whereas the smaller selenium atom is the reason for the formation of the related calcium and lead compounds.

The differences in the crystal structures of these two types of compounds are shown in Figure 5, using $PbCu_2(YO_3)_2Cl$ (Y = Se, Te) as an example. The crystal structures of $CaCu_2(SeO_3)_2Cl_2$ and $PbCu_2(SeO_3)_2Cl_2$ contain two different copper atoms in a strongly squeezed tetrahedral $[CuO_4]$ and octahedral $[CuO_4Cl_2]$ environments. In the case of octahedrally coordinated copper atoms, two oxygen atoms are situated at distances about 2.6 Å and $[CuO_2Cl_2]$ may be considered as a magnetic plaquette. Calcium or lead atoms are situated in the 8-vertex polyhedrons $[MO_4Cl_4]$. Selenium atoms share common O vertexes of copper and calcium or lead polyhedra and are situated next to the holes of the framework formed by them. From data presented in [28,29] it may be seen that Cu–Cu distances are relatively long. In case of the Ca compound the distances are 3.85–4.12 Å, and for the Pb compound the distances are 3.93–4.06 Å.

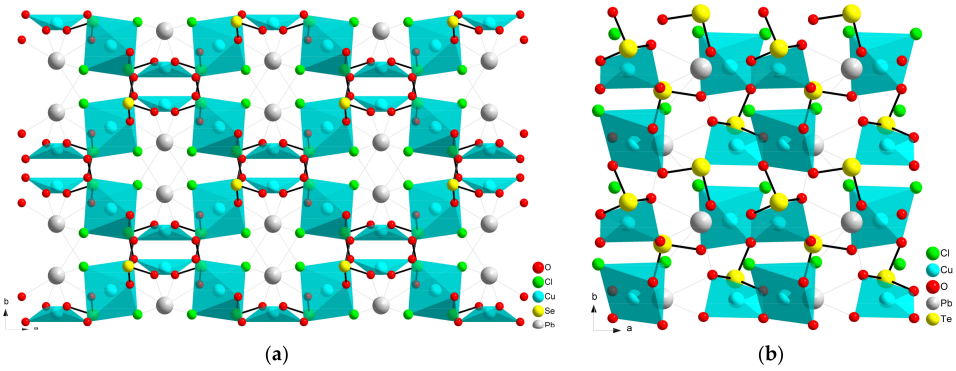

Figure 5. Copper polyhedra in the crystal structures of $PbCu_2(SeO_3)_2Cl$ (**a**) and $PbCu_2(TeO_3)_2Cl$ (**b**).

Within this wide variety of compositions, magnetic properties are known only for $CaCu_2(SeO_3)_2Cl_2$ [28], $PbCu_2(SeO_3)_2Cl_2$ [29], $SrCu_2(SeO_3)_2Cl_2$, and $Sr_2Cu(SeO_3)_2Cl_2$ [46]. Results of magnetic susceptibility measurements in the wide temperature range for $CaCu_2(SeO_3)_2Cl_2$ indicate the low-dimensional character of magnetic behavior with predominant antiferromagnetic interactions for this compound (Figure 6). Antiferromagnetic ordering takes place at approximately 6 K. The $\chi(T)$ curve approximation resulted in a uniform spin-1/2 chain model for the magnetic structure. A strong intrachain exchange coupling of ~133 K and frustrated interchain couplings realized via the two non-equivalent superexchange paths take place in the magnetic structure (Figure 7). It is worth mentioning that structural and magnetic chains are not the same in $CaCu_2(SeO_3)_2Cl_2$: due to the peculiar crystal structure, the spin chains run in the direction almost perpendicular to that of the structural chains (Figure 8).

$PbCu_2(SeO_3)_2Cl_2$ is isostructural to $CaCu_2(SeO_3)_2Cl_2$ and its magnetic behavior is somewhat similar to that of the calcium compound (Figure 9). It can be approximated by a uniform spin-1/2 chain model with interchain interactions. As in the calcium compound, magnetic chains do not coincide with the structural ones (Figure 10). However, the interchain couplings in $PbCu_2(SeO_3)_2Cl_2$ and $CaCu_2(SeO_3)_2Cl_2$ are rather different: the larger value of the interchain exchange integral in $PbCu_2(SeO_3)_2Cl_2$ results in an increase of Neel temperature (13 K in $PbCu_2(SeO_3)_2Cl_2$ versus 6 K in $CaCu_2(SeO_3)_2Cl_2$).

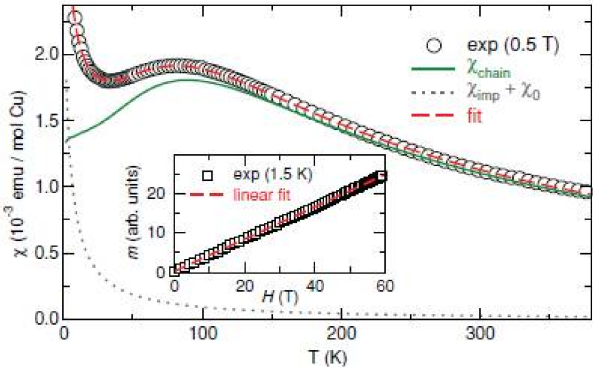

Figure 6. Magnetic susceptibility measured for $CaCu_2(SeO_3)_2Cl_2$ (circles) and the uniform spin-1/2 chain model fit (dashed line). Heisenberg chain (solid line) and impurity (dotted line) contributions to the fitted curve are shown. The inset shows the high-field magnetization curve (squares) with a linear fit (dashed line) Reprinted figure with permission from [28] Copyright (2011) by the American Physical Society.

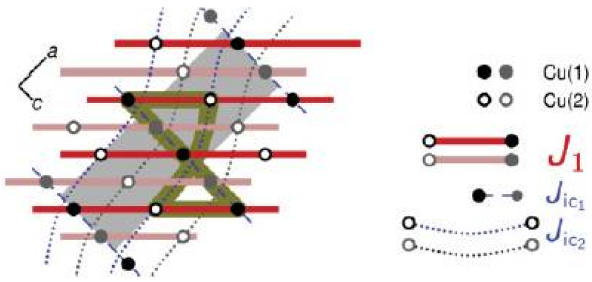

Figure 7. Spin model for $CaCu_2(SeO_3)_2Cl_2$. Filled and empty circles show the Cu(1) and Cu(2) positions, respectively. Bold lines and circles denote atoms in the front plane, whereas gray circles and shaded lines correspond to the atoms lying in the back plane. The planes are connected by Jic1 couplings only. A closed loop (bold line) having an odd number of AFM couplings indicates that the spin model is frustrated. The unit cell is depicted by the gray rectangle. Reprinted figure with permission from [28] Copyright (2011) by the American Physical Society.

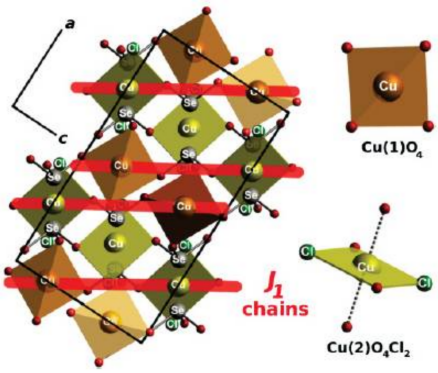

Figure 8. (left) Crystal structure of $CaCu_2(SeO_3)_2Cl_2$. The structural chains run along [10¯1] (not shown), whereas the magnetic chains range along ∼[201], as shown by bold (red) lines. Small unlabeled spheres denote O atoms. (right) Local environment of Cu(1) and Cu(2). The magnetically active Cu(1)O_4 and Cu(2)O_2Cl_2 plaquettes are highlighted. Reprinted figure with permission from [28] Copyright (2011) by the American Physical Society.

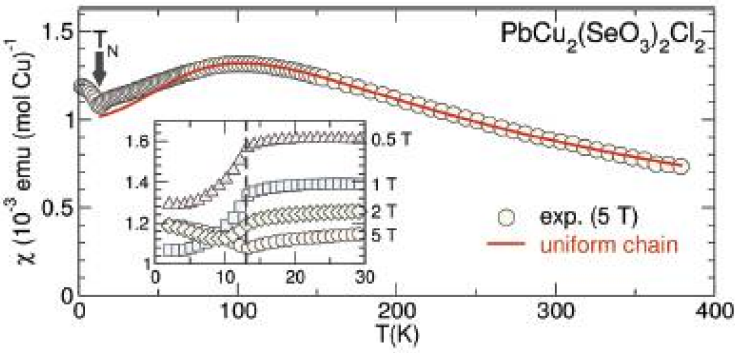

Figure 9. Magnetic susceptibility of $PbCu_2(SeO_3)_2Cl_2$ (circles) and the fit (solid line) using a uniform Heisenberg chain model with J_1 = 160 K, g = 1.97, and the temperature independent contribution $\chi_0 = 2 \times 10^{-5}$ emu (mol Cu)$^{-1}$. The kink at 13 K indicates long-range magnetic ordering. Inset: field dependence of χ(T). The strong dependence of χ on the magnetic field above T_N is an extrinsic effect (ferromagnetic impurity). Reproduced from Ref. [29] with permission from the Royal Society of Chemistry.

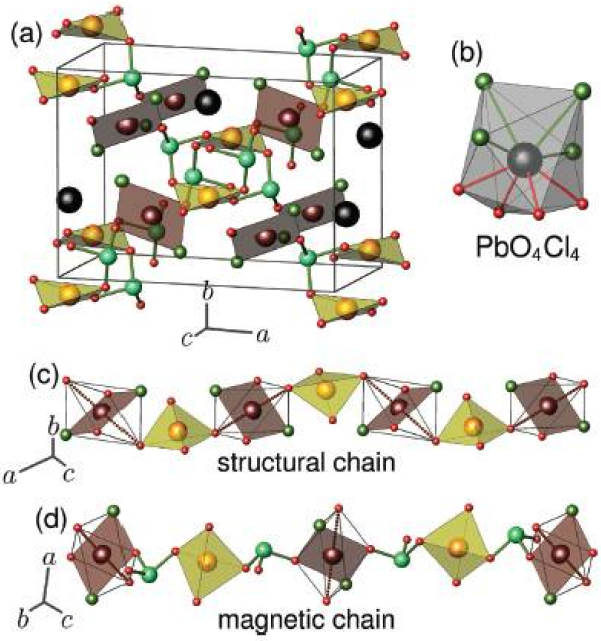

Figure 10. Crystal structure of $PbCu_2(SeO_3)_2Cl_2$. (**a**) The unit cell. Magnetic $Cu(1)O_4$ and $Cu(2)O_2Cl_2$ plaquettes are shown as light and dark filled polyhedra. Se–O bonds and Pb atoms are denoted by lines and large black spheres, respectively. (**b**) The coordination polyhedron of Pb. (**c**) Structural chains, formed by cornersharing $Cu(1)O_4$ distorted plaquettes and $Cu(2)O_4Cl_2$ octahedra (empty octahedra, with filled $Cu(2)O_2Cl_2$ plaquettes; long Cu(2)-O contacts are shown with thick dashed lines). (**d**) Magnetic chains. The nearest-neighbor superexchange J_1 runs via Cu(1)–O$\cdots$O–Cu(2) paths, along the edge of a SeO_3 pyramid (Se–O bonds are shown with lines). Reproduced from Ref. [29] with permission from the Royal Society of Chemistry.

Though $Sr_2Cu(SeO_3)_2Cl_2$ has a different structure from MM″$(SeO_3)_2Cl_2$ compounds, its magnetic behavior can also be described in terms of the Heisenberg uniform spin chain with strong interchain interactions (J $\approx$ 104–106 K). Unlike $CaCu_2(SeO_3)_2Cl_2$ and $PbCu_2(SeO_3)_2Cl_2$, in $Sr_2Cu(SeO_3)_2Cl_2$ there is presumably no long-range order observed down to at least 2 K, and magnetic exchange paths lie through the structural chains built of copper polyhedra and SeO_3^{2-} groups [46]. Further

investigation is needed to establish the microscopic magnetic model and to define exchange paths in the magnetic subsystem.

A different case is with $SrCu_2(SeO_3)_2Cl_2$. Here, the most appropriate model is the one of slightly interacting dimers. This is due to the structural features including CuO_4 corner-shared plaquettes. In general, according to preliminary measurements data the magnetic behavior of $SrCu_2(SeO_3)_2Cl_2$ is similar to that of $SrCu_2(TeO_3)_2Cl_2$. Nevertheless, further research should be undertaken in order to reveal special features inherent to this phase.

2.3. Compound $Bi_2Fe(SeO_3)_2OCl_3$

As seen from the above-mentioned data, the majority of selenite halides with described magnetic properties were studied in compounds featuring copper in the oxidation state 2+ which have S = 1/2. An example of a compound where ions with larger spin values may form magnetic sublattice is selenite oxochloride of iron and bismuth $Bi_2Fe(SeO_3)_2OCl_3$ [30] (Table 1 compound 12). The main feature of the crystal structure of this compound is the existence of the zig-zag chains of corner-shared $[FeO_6]$ octahedra which are decorated by $[BiO_4Cl_3]$, $[BiO_3Cl_3]$ polyhedra and SeO_3^{2-} groups as shown in Figure 11. The selenium atoms are connected to the oxygen atoms from different $[FeO_6]$ octahedra and an additional link chain. Different iron octahedron chains are bound by Bi-polyhedra into the layer in the ab plane of the structure as depicted in Figure 11. Finally, the distance between nearest Fe^{3+} ions in the chain is about 3.56 Å and between Fe^{3+} ions from different chains and layers are 8.570(2) and 8.604(2) Å. According to this structure's peculiarity, it may be suggested that the compound will be magnetically quasi-one-dimensional.

An extensive study is required to establish the character of magnetic behavior in this compound. The temperature dependence of magnetic susceptibility displays broad maximum at T ≈ 130 K, which indicates the formation of the short-range magnetic order (Figure 12). At lower temperature T_N = 13 K, long-range antiferromagnetic ordering sets in, and this is confirmed by means of magnetization and specific heat measurements as well as by Mössbauer spectra. ESR spectroscopy data point out the quasi-1D nature of magnetic interactions. The first-principle calculations allowed defining of the main spin-exchange paths in the magnetic structure based on weakly interacted spin-5/2 zig-zag chains with strong intrachain interactions (Figure 13). Thus, a compound with a higher spin magnetic system has been demonstrated to be a low-dimensional magnet.

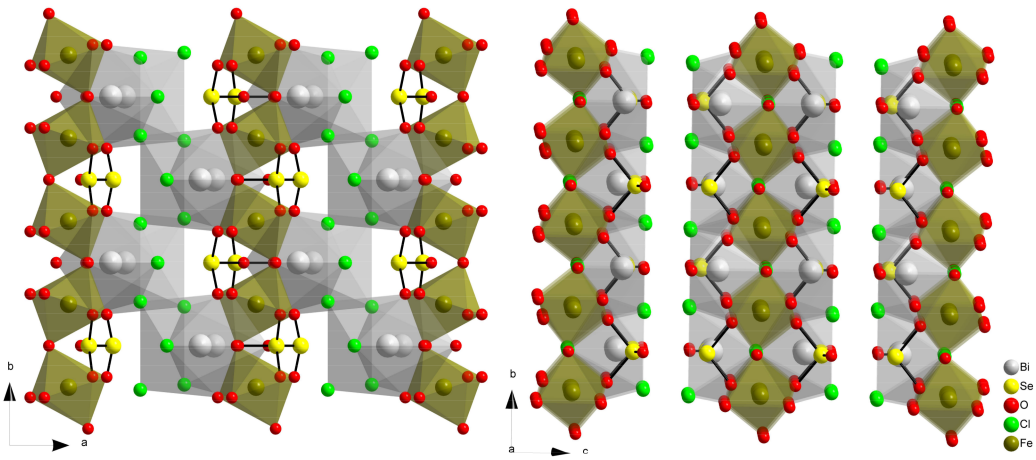

Figure 11. The view on $[FeO_6]$ octahedra chains decorated by Bi polyhedra and SeO_3^{2-} groups in the crystal structure of $Bi_2Fe(SeO_3)_2OCl_3$.

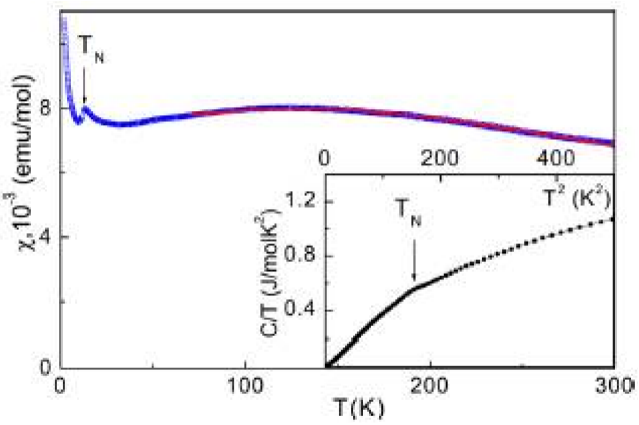

Figure 12. Temperature dependence of magnetic susceptibility in $Bi_2Fe(SeO_3)_2OCl_3$. The solid line represents the fit in a Heisenberg S = ∞ antiferromagnetic chain model. The inset represents the temperature dependence of specific heat on the C/T vs. T^2 scale. Reprinted with permission from [30] Copyright (2014) American Chemical Society.

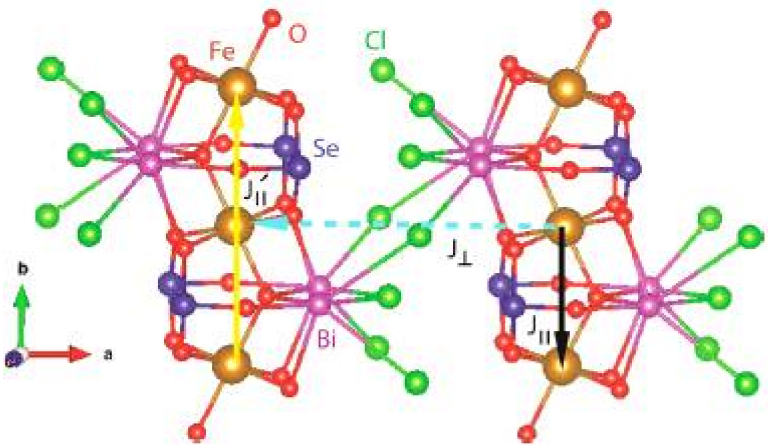

Figure 13. Exchange paths for various magnetic interactions $J_{\parallel}$ (in black), $J_{\parallel}'$ (in cyan), and $J_{\perp}$ (in gold) in $Bi_2Fe(SeO_3)_2OCl_3$. Reprinted with permission from [30]. Copyright (2014) American Chemical Society.

2.4. Francisite Like Compounds $Cu_3M(SeO_3)_2O_2X$

The Table 1 shows that the most representative group of compounds with the same structure symmetry and relative cell constants is formed by compounds with common composition $Cu_3M(SeO_3)_2O_2X$ [31–37] (Compounds 13–30 Table 1). All these compounds are isostructural to the rare nature mineral Francisite $Cu_3Bi(SeO_3)_2O_2Cl$ [47]. Later, its synthetic analogs for Cl, Br, and I were prepared in laboratory conditions [31]. It was shown that rare Earth metals may form compounds with francisite-like structures [32–36]. The crystal structure of francisite contains two copper ions positions with square planar oxygen atom coordination. Bismuth or rare Earth metal ions are in distorted cubic surroundings [MO_8]. The square planes [CuO_4] form kagome-like nets in the crystal structure (Figure 14). As can be seen in the Figure 14 selenite groups connect [CuO_4] planes and [MO_8] cubes into the 3D framework with the channels running along [0 0 1] direction. Halide atoms are situated inside these channels. The nearest distance from Cl atom is Cu–Cl which is more than 3 Å for $Cu_3Bi(SeO_3)_2O_2Cl$ (Figure 14). The most recent studies have shown that francisite-like compounds may be formed for all are Earth Metals from La up to Lu and Y in case of chlorides [35,36] and for La till Gd in case of bromides [36]. This phenomenon may be explained by the halide ion size factor where bigger bromide ions could not be combined with smaller Rare Earths and the structure could

not be formed [36]. The Kagome net in the francisite-like structures is not planar and form waves as shown in Figure 15. The main attractive structural feature of francisite-like compounds is that the variation of M^{3+} ion may affect Cu–Cu distance in the Kagome nets. One would expect that Cu–Cu contact distances should decrease with decreasing Ln^{3+} ionic radii. The experimental data summarized for chlorides in Figure 16. support such an approach but Cu1-Cu2-Cu1 angle of the net shows a more complex dependence. There are two Cu–Cu distances in the net. The Cu–Cu distances in chloride compounds are within the range of 3.13–3.23 Å. Figure 16 shows that the differences in the Cu–Cu distances decrease together with decreasing of Ln^{3+} radii. The variation of M^{3+} and of halide ions provides an opportunity for the copper sublattice tuning. Substitution of selenium by tellurium produced the compound $Cu_3Bi(TeO_3)_2O_2Cl$ [48]. However, the copper Kagome net in the tellurite is more distorted and one copper atom has become pyramidally coordinated [CuO_4Cl]. The existence of such a wide group of compounds with similar structures, together with the possibility to examine the influence of the f-element magnetic nature on the magnetic behavior of the copper ions sublattice stimulate the research of this group of substances.

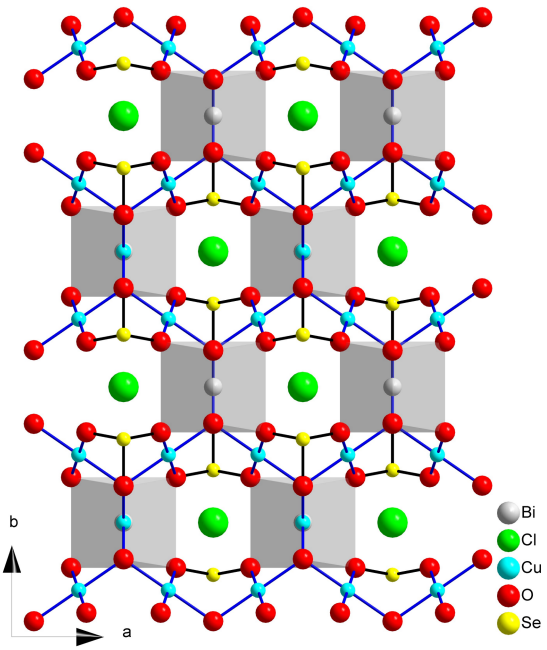

Figure 14. The crystal structure of $Cu_3Bi(SeO_3)_2Cl$. [BiO_8] distorted cubes are shown.

The discussion of the magnetic properties of the francisite family representatives should be started with the consideration of the synthetic analogs of this mineral with the composition $Cu_3Bi(SeO_3)_2O_2X$ (X = Cl, Br). According to magnetic susceptibility measurements data, antiferromagnetic ordering in spin-1/2 copper subsystem takes place at 23.5(5) K [31] and 27.4(5) K [49] for $Cu_3Bi(SeO_3)_2O_2Cl$ and $Cu_3Bi(SeO_3)_2O_2Br$, respectively. The magnetic ground state can be described as distorted kagome layers in ab plane, coupled antiferromagnetically. It should be noted that the layers exhibit a canted ferromagnetic spin arrangement. Applying an external magnetic field triggers a metamagnetic transition in both compounds (BC $\approx$ 0.8 T) [49–51]. Many research groups contributed to the studies of the microscopic magnetic structure of the synthetic francisites. These fruitful structural, electromagnetic, and optical studies combined with the theoretical calculations resulted in discoveries of some interesting features of the francisite-like compounds [49–61]. Thus, a structural transition was detected in $Cu_3Bi(SeO_3)_2O_2Cl$, but surprisingly it was not observed in $Cu_3Bi(SeO_3)_2O_2Br$. Moreover, the origin of this transition is still not clear [59–61]. The most recent publications suggest spin-flip-induced multiferroic behavior in $Cu_3Bi(SeO_3)_2O_2Cl$ [57,59] and this might be a consequence of a structural transformation. However, this requires further clarification.

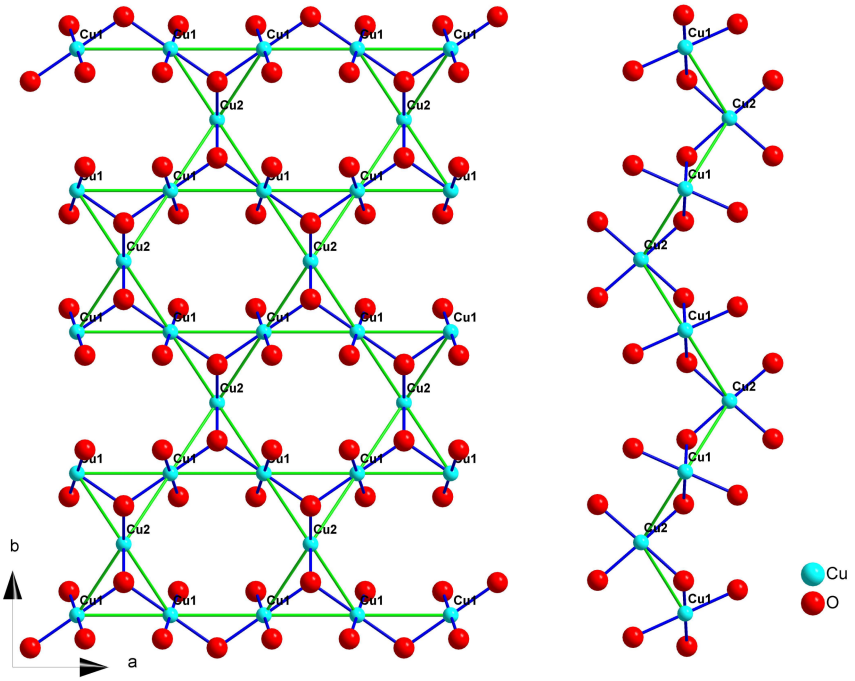

Figure 15. The copper-oxygen net in the crystal structure of Francisite-like compounds crystal structure shown in different direction. Cu–Cu contacts are marked as green. The right part of the figure shows the buckled nature of the kagome net.

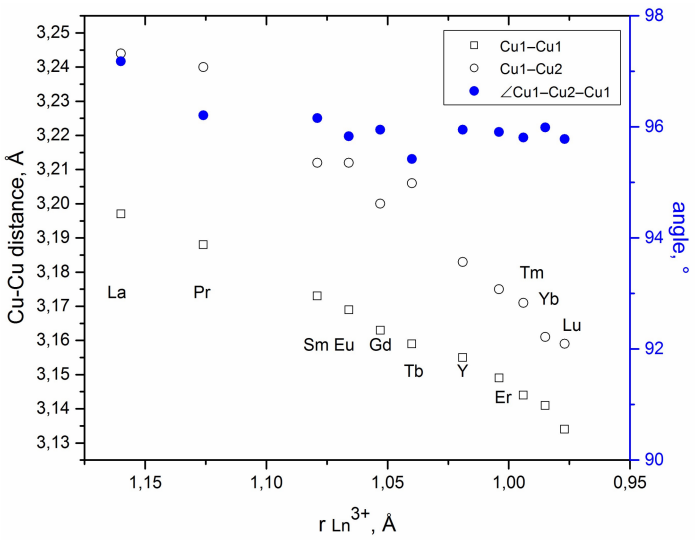

Figure 16. The variation of Cu1-Cu1, Cu1-Cu2, and ∠Cu1-Cu2-Cu1 angles as function of ionic REM radii for $Cu_3Ln(SeO_3)_2O_2Cl$ compounds.

The compounds of composition $Cu_3M(SeO_3)_2O_2X$ (M = La–Lu, X = Cl, Br) may be divided into two groups: the first one containing nonmagnetic rare earth ions such as Y^{3+}, La^{3+}, Eu^{3+}, and Lu^{3+}, and the second one featuring magnetic M^{3+} ions. Representatives of the first group demonstrate magnetic behavior similar to that of $Cu_3Bi(SeO_3)_2O_2X$ (X = Cl, Br) [32,33,35]. χ(T) and M(H) curves typical for francisite-like compounds with non-magnetic rare earth ions are shown in Figure 17. The presence of two magnetic ions in one crystal structure leads to a much more complicated magnetic behavior. It manifests itself in the appearance of the second sharp maximum on the magnetic susceptibility curve at $T < T_N$, as well as on the heat capacity temperature dependence

curve (Figure 18). Up to now a detailed study has been undertaken for only two representatives, which are $Cu_3Sm(SeO_3)_2O_2Cl$ [34] and $Cu_3Yb(SeO_3)_2O_2Cl$ [37]. In both compounds, the magnetic system undergoes the spin-reorientation transition influenced by the rare earth ion's magnetic moment. Exchange paths in the samarium compound are shown in Figure 19.

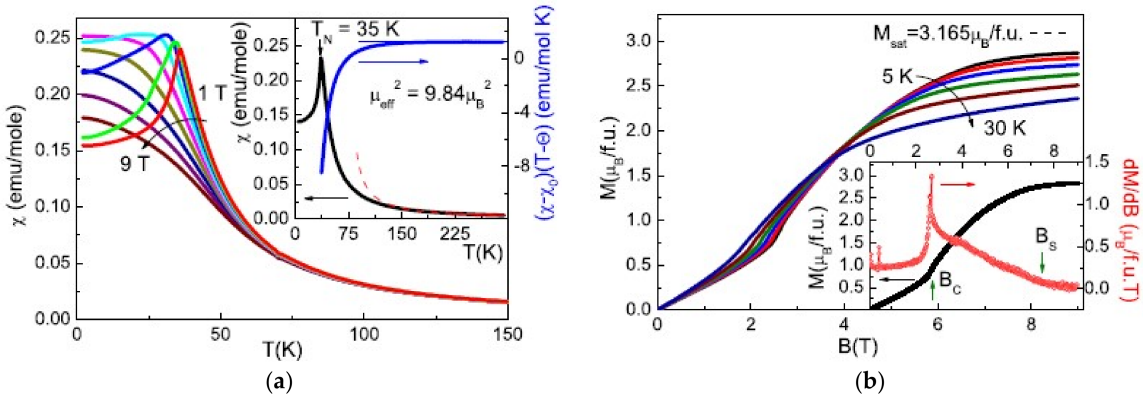

Figure 17. (**a**) The temperature dependence of the magnetic susceptibility of $Cu_3Y(SeO_3)_2O_2Cl$ at applied field strengths of 1–9 T, with a field step of 1 T. The inset represents the temperature dependence of the magnetic susceptibility at 0.1 T along with the Curie constant as a function of temperature. The dotted line represents an extrapolation of the Curie-Weiss type dependence from the high temperature region. (**b**) The field dependence of the magnetization in $Cu_3Y(SeO_3)_2O_2Cl$ over the temperature range of 5–30 K in steps of 5 K. The inset shows the field dependence of the magnetization at 2 K and its field derivative. Reprinted figure with permission from [32] Copyright (2014) by the American Physical Society.

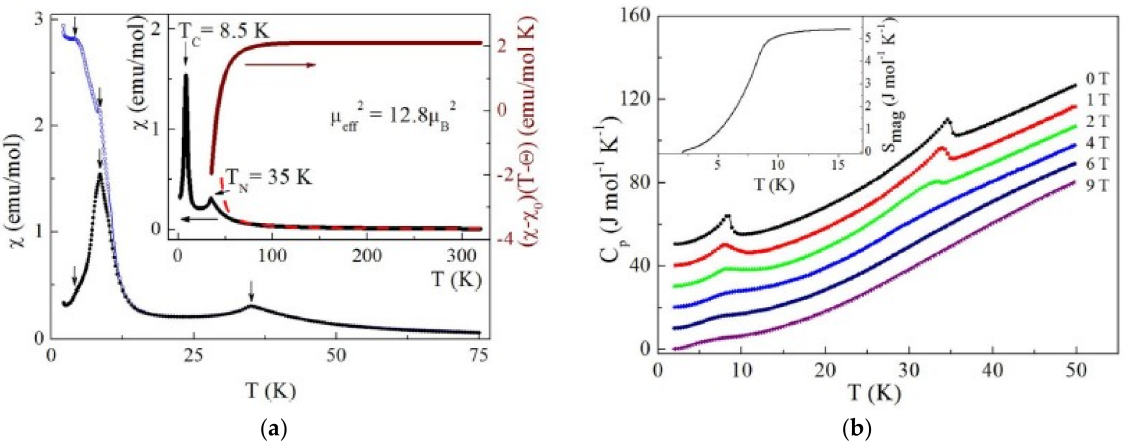

Figure 18. (**a**) The temperature dependences of magnetic susceptibility in $Cu_3Sm(SeO_3)_2O_2Cl$ in ZFC (squares) and FC (circles) regimes taken at B = 0.02 T. Inset: The ZFC curve in the range 2–320 K and its fit (dash). Also shown is the temperature dependence of Curie constant $C = (\chi - \chi_0)(T - \Theta)$. (**b**) The temperature dependences of specific heat in selected magnetic fields for $Cu_3Sm(SeO_3)_2O_2Cl$. Inset: Temperature dependence of magnetic entropy S_{mag} Reprinted figures with permission from [34]. Copyright (2016) by the American Physical Society.

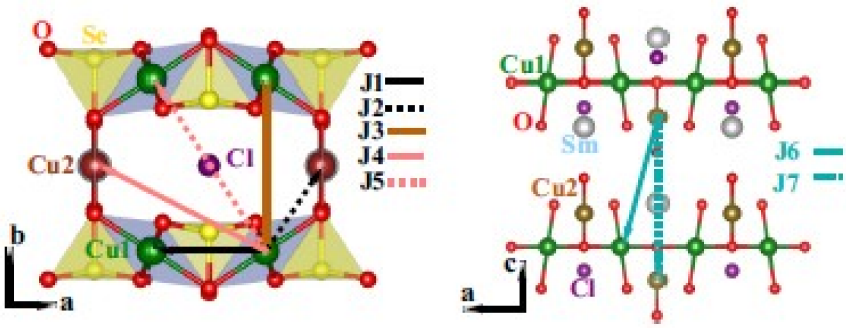

Figure 19. The exchange paths for various magnetic interactions in $Cu_3Sm(SeO_3)_2O_2Cl$. Reprinted figure with permission from [34]. Copyright (2016) by the American Physical Society.

Thus, a series of isostructural compounds have similar magnetic properties, which may be described in terms of a quasi-2D model. In all these compounds an antiferromagnetic transition in the copper subsystem occurs at $T_N \approx 31$–41 K. In case of $Cu_3M(SeO_3)_2O_2Cl$ (M = Y, La, Eu, Lu) it can be seen that the linear decrease of the ionic radii of M^{3+} leads to the decrease of the unit cell parameters (Table 1), as well as to the increase of T_N and the critical field of metamagnetic transition (Table 2). Further research in this field will enable establishing the relationships between the chemical composition, the crystal structure, and the magnetic properties of compounds in this family.

Table 2. Néel temperatures of antiferromagnetic ordering and metamagnetic transitions critical field values for $Cu_3M(SeO_3)_2O_2Cl$ (M = Y, La, Eu, Lu) and $Cu_3M(SeO_3)_2O_2Br$ (M = Bi, La).

	T_N, K	BC, T	Ref.
$Cu_3Bi(SeO_3)_2O_2Br$	27.4	0.8	[49]
$Cu_3La(SeO_3)_2O_2Cl$	31.2	2.4	[33]
$Cu_3La(SeO_3)_2O_2Br$	34.3	2.45	[33]
$Cu_3Eu(SeO_3)_2O_2Cl$	36	2.6	[35]
$Cu_3Y(SeO_3)_2O_2Cl$	36.3	2.6	[32]
$Cu_3Lu(SeO_3)_2O_2Cl$	38	3.0	[35]

2.5. Ilinskite Like Compounds $MCu_5(SeO_3)_2O_2Cl_3$

To the best of our knowledge, the most recently described group of selenite halide d-metal compounds for which structural and physical properties characterization was reported, are copper compounds with alkali metals $MCu_5(SeO_3)_2O_2Cl_3$ M = Na and K [38,39,62,63] and two isostructural halides $Na_2Cu_7(SeO_3)_4O_2X_4$ X = Cl and Br [40,64,65] while the chloride is only magnetically characterized (compounds 31–33 in Table 1). The first group comprises compounds derived from the naturally occurring mineral ilinskite $NaCu_5(SeO_3)_2O_2Cl_3$ [62]. There were obtained synthetic compounds with the same composition and structure for sodium and potassium [38,39,63]. The four copper atoms in the structure may be divided in the two types of planar coordination: $[CuO_4]$ and $[CuO_3Cl]$ (Figure 20a). In $NaCu_5(SeO_3)_2O_2Cl_3$ and $KCu_5(SeO_3)_2O_2Cl_3$ these plaquettes form well-defined layers in the *bc* plane. The layers are bridged by SeO_3^{2-} groups and interleaved by the M^+ ions. The authors of Ref. [36] reported that the pure sodium compound is less stable due to the alkali metal ion size effect. Sodium atoms have five nearest neighbors [(O + 2Cl) + 2Cl] whereas potassium is surrounded by five oxygen and four chlorine atoms. In both compounds there is a group of Cu–Cu distances in the range of 2.85–3.28 Å. The magnetic behavior of $KCu_5(SeO_3)_2O_2Cl_3$ was studied in [63] and may be described by a model of a system built by corner-sharing Cu4 tetrahedra. A part of the Cu sublattice with shortest distances is given in Figure 20b.

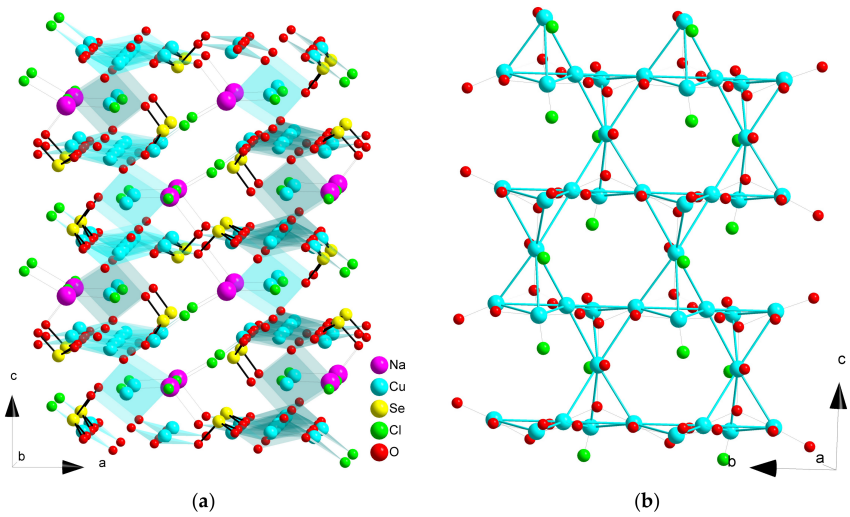

Figure 20. The crystal structure of $NaCu_5(SeO_3)_2O_2Cl_3$. Two types of $[CuO_4]$ and $[CuO_3Cl]$ plaquettes are shown (**a**); A fragment of the corner shared Cu_4 tetrahedra sublattice layer in the crystal structure of ilinskite like compounds (**b**).

In spite of the fact that the main motifs of the ilinskite structure are in general similar to those of other copper selenite halides, magnetic behavior of $KCu_5(SeO_3)_2O_2Cl_3$ is drastically different [63]. The $\chi(T)$ curve shows broad maximum at $T \approx 50$ K, but there is no evidence for any long-range order down to 2 K (Figure 21a). The absence of a λ-type anomaly on the Cp(T) curve confirms this (Figure 21b). The negative value of the Curie–Weiss temperature reflects the predominant antiferromagnetic interactions in the magnetic copper sublattice.

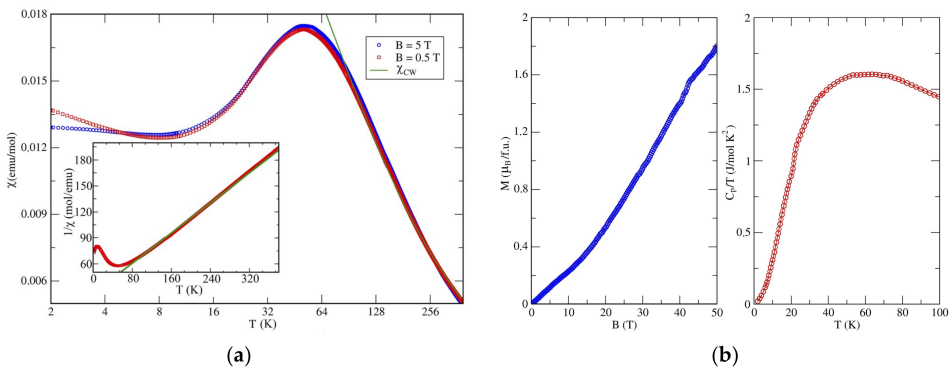

Figure 21. (**a**) Magnetic susceptibility $\chi(T)$ for $KCu_5O_2(SeO_3)_2Cl_3$ obtained at different values of the external magnetic field in the field-cooling regime. The inset shows the Curie–Weiss approximation in the 100–380 K temperature range with the parameters $\theta = 60$ K and $C = 2.3$ emu K/mol, as denoted by the green line. (**b**) The magnetization curve measured at $T = 1.5$ K. (left) Temperature dependence of the specific heat, $C_p(T)/T$, for $KCu_5O_2(SeO_3)_2Cl_3$ measured in zero field. Reproduced from [63] under Creative Commons Attribution 4.0 International License. To view a copy of this license, visit http://creativecommons.org/licenses/by/4.0/.

Application of DFT calculations combined with thermodynamic measurements resulted in a suggestion of a possible microscopic model of spin interactions in $KCu_5(SeO_3)_2O_2Cl_3$. The magnetic structure can be interpreted as layers of corner-sharing tetrahedra Cu_4 with numerous magnetic interactions between copper atoms. Most of the exchange couplings take place between nearest neighbors, and this would lead to a strong frustration effect, but the influence of non-magnetic SeO_3^{2-} groups results in the reduction of frustration. Dissimilar interactions render the system quasi-1D. Thus,

the magnetic behavior can be described in terms of non-frustrated one-dimensional units (spin ladders or tubes) with only weak and frustrated couplings between these units.

2.6. Compound $Na_2Cu_7(SeO_3)_4O_2Cl_4$

Compound $Na_2Cu_7(SeO_3)_4O_2Cl_4$ [40,65] is an example of a unique structure. There are four independent Cu crystallographic sites. These atoms form heptanuclear clusters (Figure 22 left panel). The Cu–Cu distances in the clusters are in the range of 2.96–3.25 Å. Every cluster is formed by the two tetrahedra connected by a common vertex. Copper atoms in the vertices have the square planar surrounding [CuO_4], two atoms in tetrahedra have the planar coordination [CuO_3Cl] and finally one copper atom is surrounded by four oxygen atoms and one chlorine atoms forming [CuO_4Cl] triangular bipyramid. $Na_2Cu_7(SeO_3)_4O_2Cl_4$ displays a three-dimensional network built by isolated $[Cu_7O_{14}Cl_4]^{18-}$ clusters connected by SeO_3^{2-} groups (right panel of Figure 22), in which Na^+ ions are located inside the vacancies. The same structure was found for the bromide analog $Na_2Cu_7(SeO_3)_4O_2Br_4$ [64] taking into account that Cu–O and Na–O distances are elongated compared to the chloride compound.

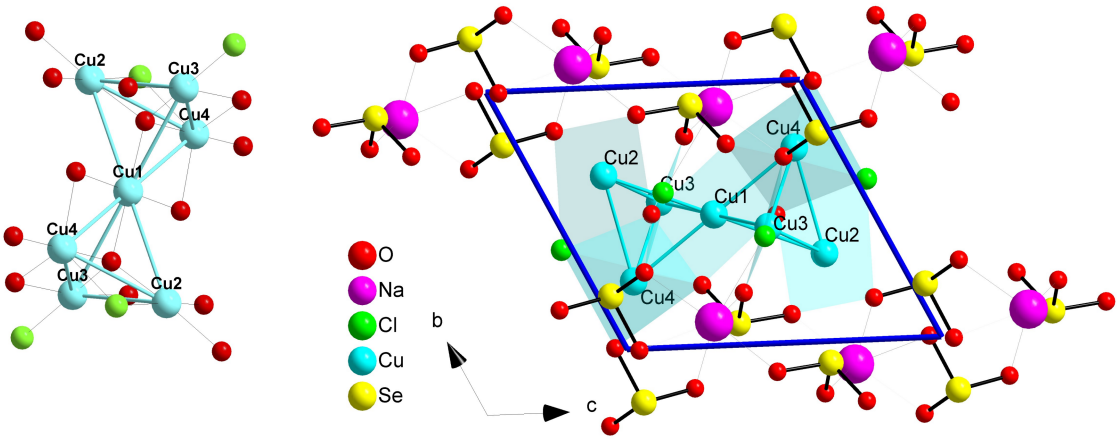

Figure 22. $[Cu_7O_{14}Cl_4]^{18-}$ cluster (left) and the copper polyhedra with SeO_3^{2-} groups in the crystal structure of $Na_2Cu_7(SeO_3)_4O_2Cl_4$ (right) [40].

In $Na_2Cu_7(SeO_3)_4O_2Cl_4$, antiferromagnetic long-range ordering takes place below $T_N \approx 5$ K. The Curie–Weiss temperature value is indicative of predominant antiferromagnetic interactions between the copper atoms. Field dependent magnetization measurements data specify the spin-flip magnetic transition. The presence of a hysteresis loop may be attributed to the ferromagnetic ground state. A magnetization plateau was observed in the magnetization curve, corresponding likely to the 3/7 magnetization plateau suggested by theoretical prediction in a reverse triangular spin-bipyramid. This data allowed proposal of a geometrical model for possible spin arrangements in magnetic sublattice.

The existence of a group with an odd number of possible spin interactions should lead to the spin-frustration effect within such groups. For $Na_2Cu_7(SeO_3)_4O_2Cl_4$ this effect was indeed found [40]. A frustration effect was evaluated using the empirical frustration parameter f:

$$\mathrm{f} = \frac{|\Theta_{CW}|}{T_N}$$

The value of f > 10 indicates a strong frustration effect. For the above-mentioned compound this value is calculated to be 13.6, and it is comparable with those calculated for similar known compounds with a magnetic frustration.

3. Conclusions and Outlook

We have attempted to show that interesting magnetic interactions in 3-D metal selenite halides appear due to the influence of lone pairs of SeO_3^{2-} groups and the affinity of halide ions to bind with metal ions instead of selenium. In addition to the described compounds there are a lot of selenite halides with promising crystal structures. Some of such compounds were mentioned by us previously. For example, the compound $Cu_5(SeO_3)_4Br_2$ [64] (Table 3) shows dimorphism and crystallizes in α form which is isostructural to $Cu_5(SeO_3)_4Cl_2$ [22] whereas β form is close to $Co_5(SeO_3)_4X_2$ X = Cl, Br [23] and $Ni_5(SeO_3)_4Br_2$ [25]. Both α and β polymorphs show 3-D Cu–Cu frameworks with Cu–Cu distances 3.16–3.61 and 3.10–3.44 Å, respectively. Such values suggest the magnetic exchange between copper ions in $Cu_5(SeO_3)_4Br_2$. A similar situation may be observed in case of $Na_2Cu_7(SeO_3)_4O_2Br_4$ [64] (Table 3), an analog of the frustrated chloride compound [40]. $Na_2Cu_7(SeO_3)_4O_2Br_4$ demonstrates the same isolated $[Cu_7O_{14}Br_4]^{18-}$ clusters with Cu–Cu distances 2.96–3.27 Å close to those in $Na_2Cu_7(SeO_3)_4O_2Cl_4$ [40].

Another alkali metal copper selenite chloride $K[Cu_3O](SeO_3)_2Cl$ [65] possesses a very interesting, unprecedented structure (Table 3). The unit cell of $K[Cu_3O](SeO_3)_2Cl$ contains three Cu^{2+} ions, two in $[CuO_4]$ plane coordination and squeezed tetrahedra and one $[CuO_4Cl]$ polyhedron. Copper atoms are situated in the range 2.94–3.35 Å and form layers in the structure of $K[Cu_3O](SeO_3)_2Cl$. The layer may be presented as formed by edge shared pairs of Cu_4 tetrahedrons which are connected into the layer in ab plane of the crystal structure Figure 23. Distances between copper atoms from different layers are about 6 Å. The system of magnetic exchange of vertex shared tetrahedra was studied in [63]. Compound $K[Cu_3O](SeO_3)_2Cl$ possess different type of tetrahedra connection but it may be expected that magnetic exchange will be found in this compound.

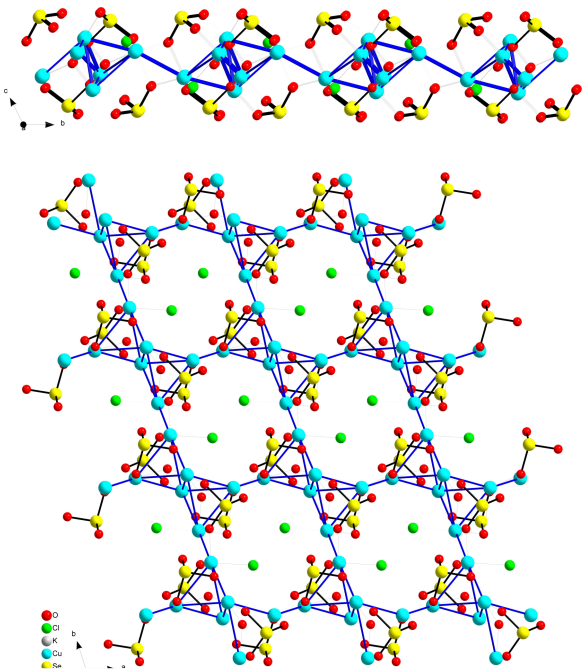

Figure 23. The presentation of the copper-oxygen layer decorated by SeO_3^{2-} groups in different directions in the crystal structure of the $K[Cu_3O](SeO_3)_2Cl$ [65]. Blue lines represent Cu–Cu contacts.

Table 3. Compositions and crystallographic data for transition metals selenite halides with possible magnetic exchange between d-metal ions.

#	Composition	Space Group	Z	Cell Constants				Ref.
				a, Å	b, Å	c, Å	Angles, °	
1	α-$Cu_5(SeO_3)_4Br_2$	$P2_1/c$	2	11.1089(18)	8.3233(13)	7.5668(12)	β = 90.893(3)	[64]
2	β-$Cu_5(SeO_3)_4Br_2$	P-1	1	6.2096(13)	7.8553(16)	7.9006(17)	α = 65.538(6) β = 83.111(7) γ = 75.291(7)	[64]
3	$Na_2Cu_7(SeO_3)_4O_2Br_4$	P-1	4	7.7657(3)	8.3750(3)	9.2626(4)	α = 110.227(2) β = 104.897(2) γ = 107.195(3)	[64]
4	$K[Cu_3O](SeO_3)_2Cl$	P-1	2	7.6821(5)	8.1179(5)	8.7836(6)	α = 113.193(3) β = 108.735(4) γ = 98.245(4)	[65]
5	$Cu_3(SeO_3)_2Cl_2$	C2/m	2	8.9333(12)	6.2164(7)	7.5815(12)	β = 110.238(13)	[66]
6	$Cu_3(SeO_3)_2Cl_2$	P-1	2	6.1240(4)	7.7880(5)	8.5170(6)	α = 92.755(4) β = 95.735(4) γ = 92.853(4)	[15]
7	$Cu_5O_2(SeO_3)_2Cl_2$	$P2_1/c$	2	6.030(1)	13.744(3)	5.562(1)	β = 95.75(1)	[67,68]
8	β-$Cu_5O_2(SeO_3)_2Cl_2$	$P2_1/c$	2	5.3982(5)	8.0543(8)	11.1277(10)	β = 99.258(2)	[69]
9	$Cu_7O_2(SeO_3)_2Cl_6$	$P2_1/c$	4	10.958(9)	14.483(5)	10.494(14)	β = 113.61(7)	[70]
10	$Cu_9O_2(SeO_3)_4Cl_6$	I2/m	2	14.170(3)	6.262(1)	12.999(3)	β = 113.05(1)	[71,72]
11	$Cu_9O_2(SeO_3)_4CI_6$	$P2_1/n$	2	12.922(3)	6.262(2)	14.042(4)	β = 112.88(2)	[73]
12	$Cu^{I}Cu^{II}{}_4O(SeO_3)Cl_5$	$P2_1/m$	2	9.203(3)	6.232(2)	9.557(3)	β = 91.970(8)	[74]
13	$Co_4(SeO_3)_3Cl_2$	Pnma	4	7.9751(1)	14.4048(2)	9.7103(2)		[75]
14	$Co_3(Se_2O_5)_2Cl_2$	C2/m	2	7.1973(10)	13.9961(19)	5.8334(9)	β = 107.524(16)	[75]
15	$Ba_2Co(SeO_3)_2Cl_2$	Pnnm	2	6.7635(4)	12.6454(7)	5.3866(3)		[76]
16	$Fe_6Ca_2(SeO_3)_9Cl_4$	$P6_3/m$	2	12.118(2)		12.703(4)		[77]
17	$CoNd_{10}(SeO_3)_{12}Cl_8$	P2/c	4	15.699(2)	15.7002(2)	19.171(2)	β = 113,995(5)	[78]

Table 3. *Cont.*

#	Composition	Space Group	Z	Cell Constants				Ref.
				a, Å	b, Å	c, Å	Angles, °	
18	$CoSm(SeO_3)_2Cl$	P-1	4	7.123(1)	8.8895(2)	12.162(2)	α = 72.25(1) β = 71.27(1) γ = 72.08(1)	[79]
19	$CuGd(SeO_3)_2Cl$	P-1	4	7.043(4)	9.096(4)	12.010(7)	α = 70.84(4) β = 73.01(4) γ = 70.69(4)	[79]
20	$MnSm(SeO_3)_2Cl$	P-1	2	7.008(2)	7.241(2)	8.034(2)	α = 86.90(3) β = 71.57(3) γ = 64.33(3)	[79]
21	$Cu^{I}Cu^{II}_5PbO_2(SeO_3)_2Cl_5$	C2/m	4	18.468(2)	6.1475(8)	15.314(2)	β = 119.284(2)	[80]
22	$KCdCu_7O_2(SeO_3)_2Cl_9$	$P6_3/mmc$	2	8.7805(8)		15.521(2)		[81]
23	$KPb_{1.5}Cu_6Zn(SeO_3)_2O_2Cl_{10}$	Pnnm	4	9.132(2)	19.415(4)	13.213(3)		[82]
24	$MnBi(SeO_3)_2Cl$	P-1	2	7.0926(8)	7.2695(6)	8.0160(8)	α = 88.226(4) β = 72.005(3) γ = 64.560(4)	[83,84]
25	$(Pb_2Cu^{2+}{}_9O_4)(SeO_3)_4(Cu^{+}Cl_2)Cl_5$	C2/m	2	18.605(17)	6.204(6)	12.673(12)	β = 109.869(17)	[85]
26	$(PbCu^{2+}{}_5O_2)(SeO_3)_2(Cu^{+}Cl_2)Cl_3$	C2/m	2	18.4956(4)	6.14540(10)	15.2985(4)	β = 119.3111(10)	[85]
27	$(Pb_xCu^{2+}{}_{(6-x)}O_2)(SeO_3)_2(Cu^{+}Cl_2)K_{(1-x)}Cl_{(4-x)}$	C2/m	1	15.1158(11)	6.1853(4)	9.2672(9)	β = 95.965(5)	[85]
28	$Pb_2VO_2(SeO_3)_2Cl$	$P2_1$	2	8.333(3)	5.3171(16)	10.710(4)	β = 111.701(5)	[86]
29	$Pb_5Cu(SeO_3)_4Cl_4$	C2/c	4	24.917(3)	5.5060(10)	14.242(2)	β = 101.770(10)	[87]

In addition to the listed compounds, some other selenite halide 3d-metals have been described in the literature and structurally characterized. These are $Cu_3(SeO_3)_2Cl_2$ [15,66], $Cu_5O_2(SeO_3)_2Cl_2$ [67–69], $Cu_7O_2(SeO_3)_2Cl_6$ [70], $Cu_9O_2(SeO_3)_4Cl_6$, [71–73], $Cu^ICu^{II}{}_4O(SeO_3)Cl_5$ [74], $Co_4(SeO_3)_3Cl_2$ [75], and the diselenite cobalt compound $Co_3(Se_2O_5)_2Cl_2$ [75]. Symmetries and cell constants for these compounds are listed in Table 3. As follows from the listed data these compounds frequently form polymorphs and some of them were found in nature as copper minerals Georgbokiite [67,68,88], Parageorgbokiite [69], Nicksobolevite [70], and Chloromenite [72] while in the laboratory conditions other crystal polymorphs may be obtained. These compounds, if they will be obtained in the phase-pure form or as crystals suitable for measurements, appear as good objects for metal–metal ions magnetic exchange studies. The majority of the listed compounds show M–M distances in the range of 2.9–3.4 Å. Taking into account these distances, a complex nature of the magnetic exchange in the compounds under consideration may be expected. From the crystallographic point of view, the most attractive compounds are layered monoclinic C2/m modifications of $Cu_3(SeO_3)_2Cl_2$ [66] and cobalt diselenite chloride $Co_3(Se_2O_5)_2Cl_2$ [75], where chains of $[CoO_4Cl_2]$ octahedra are divided by diselenite $Se_2O_5{}^{2-}$ groups in the crystal structure Figure 24. The compound $Cu^ICu^{II}{}_4O(SeO_3)Cl_5$ [74] is a good example of a structure where Cu^{2+} ions form complex chains in the crystal structure separated by chains constructed by $[Cu^ICl_3]^{2-}$ triangles, as shown in Figure 25.

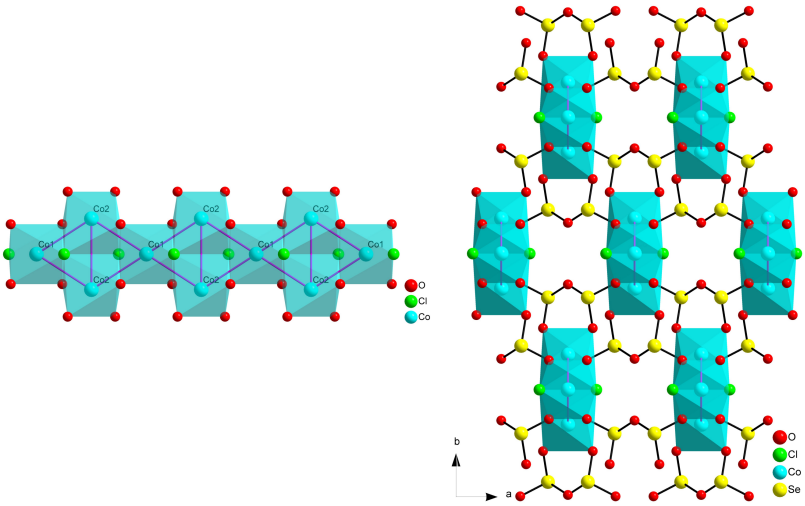

Figure 24. The chain built by $[CoO_4Cl_2]$ octahedra in the crystal structure of $Co_3(Se_2O_5)Cl_2$ (left) and view on chains interconnected by diselenite groups (right) [75].

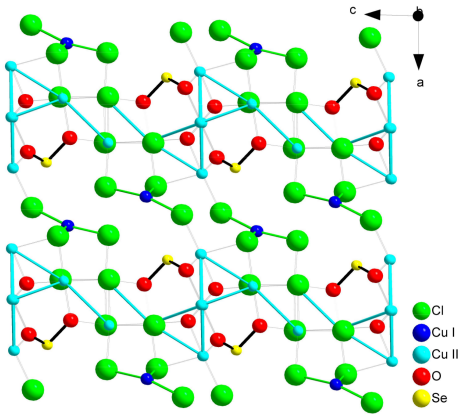

Figure 25. The complex chains of Cu^{2+} ions in the structure of $Cu^ICu^{II}{}_4O(SeO_3)Cl_5$ [74] separated by $[Cu^ICl_3]^{2-}$ groups and decorated by $SeO_3{}^{2-}$ groups.

As a 3d transition metal, zinc forms a selenite chloride known as mineral Sophiite with the composition $Zn_2(SeO_3)Cl_2$ [89] and its synthetic polymorph [90] but due to its $3d^{10}$ electron configuration it cannot possess magnetic properties.

Recently, a new tellurite-selenite chloride of iron with the composition $Fe[(Te_{1.5}Se_{0.5})O_5]Cl$ has been prepared and structurally characterized [91]. The composition of this compound is close to that of $FeTe_2O_5Cl$ [13] that shows a unique structure and possesses interesting magnetic properties, see for example [92–95]. The mixed selenite tellurite chloride of iron (III) shows the different structure [91] which is layered and contains dimers of the $[FeO_5Cl]$ octahedra, linked via common O–O edges, and mixed $[Te_3SeO_{10}]^{4-}$ tetramers. The Fe–Fe distance in the $[Fe_2O_8Cl_2]$ dimers is 3.30 Å and suggests some kind of magnetic exchange at least between Fe–Fe ions in these groups.

In addition to the above-mentioned compounds and compositions, some more complex mixed cation selenite halides have been described in the literature and may attract attention due to the possible low dimensional magnetism of 3d metal ions sublattice (Table 3 substances 15–29) [76–87]. Some of them were found in nature as minerals [80–82]. Among the listed compounds, the compounds of Mn^{2+} $MnSm(SeO_3)_2Cl$ [79] and $MnBi(SeO_3)_2Cl$ [84] deserve mentioning. The magnetic behavior of Mn^{2+} ions with S = 5/2 as well as of chromium (III) compounds in selenite halides was not described at all. To the best of our knowledge even selenites of chromium are less explored than the iron analogues. According to the literature data [96] diselenites $M_2(Se_2O_5)_3$ M = Fe, Cr crystallize in the same structures and behave as three-dimensional isotropic antiferromagnets with the weak antiferromagnetic coupling of M^{3+} ions at relatively high temperatures, but at low temperature $Fe_2(Se_2O_5)_3$ possesses a long range AF order while $Cr_2(Se_2O_5)_3$ does not, according to [96].

As was mentioned in the introduction, selenites (selenium (IV) compounds) are strong oxidants. The compound $Pb_2VO_2(SeO_3)_2Cl$ (Table 3 compound 28) [86] is the only example of vanadium selenite halides, but in this compound the V atom is in the oxidation state +5 and has no valence electrons and could not display any magnetic interaction. For this reason, there is no data about the selenite halide compounds with V or Ti in low oxidation states, as well as with Fe^{2+} or Mn^{3+}. At the same time, an anhydrous selenite of Mn(II) and Mn(III), namely, $Mn_3O(SeO_3)_3$ is known [97] suggesting the possibility to obtain manganese selenite halides. As it was demonstrated for Bi compounds with the francisite type of structures, the properties may be varied within one structure type by changing the halide ion (chloride for bromide). This serves as an attractive approach to find new compounds because bromides may sometimes show different structures and magnetic properties compared to chlorides, as evidenced for example by $Ni_5(SeO_3)_4Cl_2$ and $Ni_5(SeO_3)_4Br_2$ [24,25]. It is obvious that selenite iodides are difficult to prepare due to the possible facile oxidation of the iodide ions, but the existence of $Pb_3(SeO_3)_2I_2$ [98] and $Cu_3Bi(SeO_3)_2O_2I$ [31] demonstrates the possibility to find proper synthesis conditions and therefore opens further opportunities for future research.

The existence of the wide range of compounds for which it is possible to expect low-dimensional magnetic interactions gives reason for chemists to develop synthetic methods suitable for the preparation of these substances in the phase-pure form or as large single crystals.

In conclusion, we would like to underline again that 3d transition metal selenites, as well as closely related tellurites, are a promising and attractive family of inorganic compounds with rich crystal chemistry and possible occurrence of low-dimensional magnetic subsystems with a wide variety of topologies.

Acknowledgments: This work was supported by the Russian Foundation for Basic Research (RFBR) (Grants 16-03-00463a and 18-52-52005MHTa). S.S., University of Antwerp, and R.A.G. are acknowledged for discussion of the manuscript.

Author Contributions: All authors wrote parts of this work. P.S.B. coordinated the project.

Conflicts of Interest: The authors declare no conflict of interest.

References

1. Schiffer, P. Condensed-matter physics: Magnetic frustration squeezed out. *Nature* **2002**, *420*, 35–38. [CrossRef] [PubMed]
2. Balents, L. Spin liquids in frustrated magnets. *Nature* **2010**, *464*, 199–208. [CrossRef] [PubMed]
3. Hess, C. Heat conduction in low-dimensional quantum magnets. *Eur. Phys. J. Spec. Top.* **2007**, *151*, 73–83. [CrossRef]
4. Gillespie, R.J.; Hargittai, I. *The VSEPR Model of Molecular Geometry*; Prentice-Hall: Upper Saddle River, NJ, USA, 1991; 6990p, ISBN 978-0205123698.
5. Gillespie, R.J. The VSEPR model revisited. *Chem. Soc. Rev.* **1992**, *21*, 59–69. [CrossRef]
6. Galy, J.; Meunier, G.; Andersson, G.; Åstrtöm, A. Stéréochimie des Eléments Comportant des Paires Non Liées: Ge (II), As (III), Se(IV), Br (v), Sn (II), Sb(III), Te (IV), I (V), Xe(VI), Tl (I), Pb (II), et Bi (III) (Oxydes, Fluorures et Oxyfluorures). *J. Solid State Chem.* **1975**, *13*, 142–159. [CrossRef]
7. Mao, J.-G.; Jiang, H.-L.; Kong, F. Structures and Properties of Functional Metal Selenites and Tellurites. *Inorg. Chem.* **2008**, *47*, 8498–8510. [CrossRef] [PubMed]
8. Wickleder, M.S.; Logemann, C. Compounds Containing the Chalcogen Oxygen E–O Bond (E = S, Se, Te). In *Handbook of Chalcogen Chemistry: New Perspectives in Sulfur, Selenium and Tellurium*, 2nd ed.; Devillanova, F.A., du Mont, W.W., Eds.; RSC Publishing: Cambridge, UK, 2013; Volume 1, pp. 307–345. ISBN 978-1-84973-623-7.
9. Vanýsek, P. Electrochemical series. In *CRC Handbook of Chemistry and Physics*, 97th ed.; W.M. Haynes CRC Press: Boca Raton, FL, USA, 2016; pp. 5-78–5-84. ISBN 978-1-4987-5429-3.
10. Christy, A.G.; Mills, S.J.; Kampf, A.R. A review of the structural architecture of tellurium oxycompounds. *Mineral. Mag.* **2016**, *80*, 415–545. [CrossRef]
11. Johnsson, M.; Törnroos, K.W.; Mila, F.; Millet, P. Tetrahedral Clusters of Copper(II): Crystal Structures and Magnetic Properties of $Cu_2Te_2O_5X_2$ (X = Cl, Br). *Chem. Mater.* **2000**, *12*, 2853–2857. [CrossRef]
12. Johnsson, M.; Törnroos, K.W.; Lemmens, P.; Millet, P. Crystal Structure and Magnetic Properties of a New Two-Dimensional S = 1 Quantum Spin System $Ni_5(TeO_3)_4X_2$ (X = Cl, Br). *Chem. Mater.* **2003**, *15*, 68–73. [CrossRef]
13. Becker, R.; Johnsson, M.; Kremer, R.K.; Klauss, H.-H.; Lemmens, P. Crystal Structure and Magnetic Properties of $FeTe_2O_5X$ (X = Cl, Br): A Frustrated Spin Cluster Compound with a New Te(IV) Coordination Polyhedron. *J. Am. Chem. Soc.* **2006**, *128*, 15469–15475. [CrossRef] [PubMed]
14. Becker, R.; Johnsson, M.; Kremer, R.; Lemmens, P. Crystal structure and magnetic properties of $Cu_3(TeO_3)_2Br_2$—A layered compound with a new Cu(II) coordination polyhedron. *J. Solid State Chem.* **2005**, *178*, 2024–2029. [CrossRef]
15. Millet, P.; Bastide, B.; Johnsson, M. $Cu_3(SeO_3)_2Cl_2$: A new oxochloride of copper(II) and selenium(IV). *Solid State Commun.* **2000**, *113*, 719–723. [CrossRef]
16. Lemmens, P.; Millet, P. Spin—Orbit—Topology, a triptych. In *Quantum Magnetism*; Lecture Notes in Physics; Schollwöck, U., Richter, J., Farnell, D.J.J., Bishop, R.F., Eds.; Springer: Berlin/Heidelberg, Germany, 2004; Volume 645, pp. 433–477. ISBN 978-3-540-40066-0. [CrossRef]
17. Cao, X.-L.; Hu, C.-L.; Xu, X.; Kong, F.; Mao, J.-G. $Pb_2TiOF(SeO_3)_2Cl$ and $Pb_2NbO_2(SeO_3)_2Cl$: Small changes in structure induced a very large SHG enhancement. *Chem. Commun.* **2013**, *49*, 9965–9967. [CrossRef] [PubMed]
18. Hu, S.; Johnsson, M.; Law, J.M.; Bettis, J.L., Jr.; Whangbo, M.-H.; Kremer, R.K. Crystal Structure and Magnetic Properties of the S = 1/2 Quantum Spin System $Cu_7(TeO_3)_6F_2$ with Mixed Dimensionality. *Inorg. Chem.* **2014**, *53*, 4250–4256. [CrossRef] [PubMed]
19. Hu, S.; Johnsson, M. Synthesis and crystal structure of two synthetic oxofluoride framework compounds—$Co_2TeO_3F_2$ and $Co_2SeO_3F_2$. *Dalton Trans.* **2012**, *41*, 12786–12789. [CrossRef] [PubMed]
20. Orive, J.; Balda, R.; Fernández, J.; Lezamad, L.; Arriortua, M.I. Low temperature red luminescence of a fluorinated Mn-doped zinc selenite. *Dalton Trans.* **2013**, *42*, 12481–12494. [CrossRef] [PubMed]
21. Liang, M.-L.; Ma, Y.-X.; Hu, C.-L.; Kong, F.; Mao, J.-G. $A(VO_2F)(SeO_3)$ (A = Sr, Ba) and $Ba(MOF_2)(TeO_4)$ (M = Mo, W): First examples of alkali-earth selenites/tellurites with a fluorinated d^0-TM octahedron. *Dalton Trans.* **2018**, *47*, 1513–1519. [CrossRef] [PubMed]

22. Zhang, D.; Berger, H.; Kremer, R.K.; Wulferding, D.; Lemmens, P.; Johnsson, M. Synthesis, Crystal Structure, and Magnetic Properties of the Copper Selenite Chloride $Cu_5(SeO_3)_4Cl_2$. *Inorg. Chem.* **2010**, *49*, 9683–9688. [CrossRef] [PubMed]
23. Becker, R.; Prester, M.; Berger, H.; Lin, P.H.; Johnsson, M.; Drobac, D.; Zivkovic, I. Crystal structure and magnetic properties of two new cobalt selenite halides: $Co_5(SeO_3)_4X_2$ (X = Cl, Br). *J. Solid State Chem.* **2007**, *180*, 1051–1059. [CrossRef]
24. Shen, Y.-L.; Mao, J.-G.; Jiang, H.-L. Synthesis, crystal structure and magnetic property of a new nickel selenite chloride: $Ni_5(SeO_3)_4Cl_2$. *J. Solid State Chem.* **2005**, *178*, 2942–2946. [CrossRef]
25. Jiang, H.-L.; Mao, J.-G. New Members in the $Ni_{n+1}(QO_3)_nX_2$ Family: Unusual 3D Network Based on Ni_4ClO_3 Cubane-like Clusters in $Ni_7(TeO_3)_6Cl$. *Inorg. Chem.* **2006**, *45*, 7593–7599. [CrossRef] [PubMed]
26. Berdonosov, P.S.; Olenev, A.V.; Kuznetsov, A.N.; Dolgikh, V.A. A group of new selenite-chlorides of strontium and d-metals (Co, Ni): Synthesis, thermal behavior and crystal chemistry. *J. Solid State Chem.* **2009**, *182*, 77–82. [CrossRef]
27. Berdonosov, P.S.; Olenev, A.V.; Dolgikh, V.A. Strontium–copper selenite–chlorides: Synthesis and structural investigation. *J. Solid State Chem.* **2009**, *182*, 2368–2373. [CrossRef]
28. Janson, O.; Tsirlin, A.A.; Osipova, E.S.; Berdonosov, P.S.; Olenev, A.V.; Dolgikh, V.A.; Rosner, H. $CaCu_2(SeO_3)_2Cl_2$: Spin-1/2 Heisenberg chain compound with complex frustrated interchain couplings. *Phys. Rev.* **2011**, *B83*, 144423. [CrossRef]
29. Berdonosov, P.S.; Janson, O.; Olenev, A.V.; Krivovichev, S.V.; Rosner, H.; Dolgikh, V.A.; Tsirlin, A.A. Crystal structures and variable magnetism of $PbCu_2(XO_3)_2Cl_2$ with X = Se, Te. *Dalton Trans.* **2013**, *42*, 9547–9554. [CrossRef] [PubMed]
30. Berdonosov, P.S.; Kuznetsova, E.S.; Dolgikh, V.A.; Sobolev, A.V.; Presniakov, I.A.; Olenev, A.V.; Rahaman, B.; Saha-Dasgupta, T.; Zakharov, K.V.; Zvereva, E.A.; et al. Crystal Structure, Physical Properties, and Electronic and Magnetic Structure of the Spin S = 5/2 Zigzag Chain Compound $Bi_2Fe(SeO_3)_2OCl_3$. *Inorg. Chem.* **2014**, *53*, 5830–5838. [CrossRef] [PubMed]
31. Millet, P.; Bastide, B.; Pashchenko, V.; Gnatchenko, S.; Gapon, V.; Ksarid, Y.; Stepanov, A. Syntheses, crystal structures and magnetic properties of francisite compounds $Cu_3Bi(SeO_3)_2O_2X$ (X = Cl, Br and I). *J. Mater. Chem.* **2001**, *11*, 1152–1157. [CrossRef]
32. Zakharov, K.V.; Zvereva, E.A.; Berdonosov, P.S.; Kuznetsova, E.S.; Dolgikh, V.A.; Clark, L.; Black, C.; Lightfoot, P.; Kockelmann, W.; Pchelkina, Z.V.; et al. Thermodynamic properties, electron spin resonance, and underlying spin model in $Cu_3Y(SeO_3)_2O_2Cl$. *Phys. Rev.* **2014**, *B90*, 214417. [CrossRef]
33. Markina, M.M.; Zakharov, K.V.; Zvereva, E.A.; Denisov, R.S.; Berdonosov, P.S.; Dolgikh, V.A.; Kuznetsova, E.S.; Olenev, A.V.; Vasiliev, A.N. Static and dynamic magnetic properties of two synthetic francisites $Cu_3La(SeO_3)_2O_2X$ (X = Br and Cl). *Phys. Chem. Miner.* **2017**, *44*, 277–285. [CrossRef]
34. Zakharov, K.V.; Zvereva, E.A.; Markina, M.M.; Stratan, M.I.; Kuznetsova, E.S.; Dunaev, S.F.; Berdonosov, P.S.; Dolgikh, V.A.; Olenev, A.V.; Klimin, S.A.; et al. Magnetic, resonance, and optical properties of $Cu_3Sm(SeO_3)_2O_2Cl$: A rare-earth francisite compound. *Phys. Rev.* **2016**, *B94*, 054401. [CrossRef]
35. Zakharov, K.V.; Zvereva, E.A.; Kuznetsova, E.S.; Berdonosov, P.S.; Dolgikh, V.A.; Markina, M.M.; Olenev, A.V.; Shakin, A.A.; Volkova, O.S.; Vasiliev, A.N. Two new lanthanide members of francisite family $Cu_3Ln(SeO_3)_2O_2Cl$ (Ln = Eu, Lu). *J. Alloys Comp.* **2016**, *685*, 442–447. [CrossRef]
36. Berdonosov, P.S.; Dolgikh, V.A. Copper Lanthanide Selenite Oxohalides with Francisite Structure: Synthesis and Structural Characteristics. *Russ. J. Inorg. Chem.* **2008**, *53*, 1353–1358. [CrossRef]
37. Markina, M.M.; Zakharov, K.V.; Ovchenko, E.A.; Berdonosov, P.S.; Dolgikh, V.A.; Kuznetsova, E.S.; Olenev, A.V.; Klimin, S.A.; Kashchenko, M.A.; Budkin, I.V.; et al. Interplay of rare-earth and transition-metal subsystems in $Cu_3Yb(SeO_3)_2O_2Cl$. *Phys. Rev.* **2017**, *B94*, 134422. [CrossRef]
38. Krivovichev, S.V.; Filatov, S.K.; Vergasova, L.P. The crystal structure of ilinskite, $NaCu_5O_2(SeO_3)_2Cl_3$, and review of mixed-ligand CuO_mCl_n coordination geometries in minerals and inorganic compounds. *Miner. Petrol.* **2013**, *107*, 235–242. [CrossRef]
39. Kovrugin, V.M.; Siidra, O.I.; Colmont, M.; Mentré, O.; Krivovichev, S.V. Emulating exhalative chemistry: Synthesis and structural characterization of ilinskite, $Na[Cu_5O_2](SeO_3)_2Cl_3$, and its K-analogue. *Miner. Petrol.* **2015**, *109*, 421–430. [CrossRef]

40. Tang, Y.; Guo, W.; Zhang, S.; Xiang, H.; Cui, M.; He, Z. $Na_2Cu_7(SeO_3)_4O_2Cl_4$: A selenite chloride compound with Cu7 units showing spin-frustration and a magnetization plateau. *Dalton Trans.* **2016**, *45*, 8324–8326. [CrossRef] [PubMed]
41. Yun, Y.; Wan, W.; Rabbani, F.; Su, J.; Xu, H.; Hovmöler, S.; Johnsson, M.; Zou, X. Phase identification and structure determination from multiphase crystalline powder samples by rotation electron diffraction. *J. Appl. Cryst.* **2014**, *47*, 2048–2054. [CrossRef]
42. Becker, R.M.; Prester, H.; Berger, M.; Johnsson, D.; Drobac, I. Zivkovic Crystal structure and magnetic properties of the new cobalt tellurite halide $Co_5(TeO_3)_4X_2$ (X = Cl, Br). *Solid State Sci.* **2007**, *9*, 223–230. [CrossRef]
43. Takagi, R.; Johnsson, M.; Kremer, R.K.; Lemmens, P. Crystal structure and magnetic properties of the coupled spin dimer compound $SrCu_2(TeO_3)_2Cl_2$. *J. Solid State Chem.* **2006**, *179*, 3763–3767. [CrossRef]
44. Feger, C.R.; Kolis, J.W. Synthesis and Characterization of Two New Copper Tellurites, $Ba_2Cu_4Te_4O_{11}Cl_4$ and $BaCu_2Te_2O_6Cl_2$, in Supercritical H_2O. *Inorg. Chem.* **1998**, *37*, 4046–4051. [CrossRef] [PubMed]
45. Shannon, R.D. Revised effective ionic radii and systematic studies of interatomic distances in halides and chalcogenides. *Acta Cryst.* **1976**, *A32*, 751–767. [CrossRef]
46. Berdonosov, P.S.; Dolgikh, V.A.; Tsirlin, A.A.; Janson, O. Copper(II) selenate(IV) chlorides as low-dimensional magnets. In Proceedings of the 18th International Conference on Solid Compounds of Transition Elements, Lisbon, Portugal, 31 March–5 April 2012; p. 215.
47. .Pring, A.; Gatehouse, B.M.; Birch, W.D. Francisite, $Cu_3Bi(SeO_3)_2O_2Cl$, a new mineral from Iron Monarch, South Australia: Description and crystal structure. *Am. Mineral.* **1990**, *75*, 1421–1425.
48. Becker, R.; Johnsson, M. Crystal structure of $Cu_3Bi(TeO_3)_2O_2Cl$: A Kagomé lattice type compound. *Solid State Sci.* **2006**, *7*, 375–380. [CrossRef]
49. Pregelj, M.; Zaharko, O.; Günther, A.; Loidl, A.; Tsurkan, V.; Guerrero, S. Magnetic ground state and two-dimensional behavior in pseudo-kagome layered system $Cu_3Bi(SeO_3)_2O_2Br$. *Phys. Rev. B* **2012**, *86*, 144409. [CrossRef]
50. Miller, K.H.; Stephens, P.W.; Martin, C.; Constable, E.; Lewis, R.A.; Berger, H.; Carr, G.L.; Tanner, D.B. Infrared phonon anomaly and magnetic excitations in single-crystal $Cu_3Bi(SeO_3)_2O_2Cl$. *Phys. Rev.* **2012**, *B86*, 174104. [CrossRef]
51. Nikolaev, S.A.; Mazurenko, V.V.; Tsirlin, A.A.; Mazurenko, V.G. First-principles study of the magnetic ground state and magnetization process of the kagome francisites $Cu_3Bi(SeO_3)_2O_2X$ (X = Cl, Br). *Phys. Rev.* **2016**, *B94*, 144412. [CrossRef]
52. Miller, K.H.; Constable, E.; Berger, H.; Tanner, D.B.; Horvat, J. Complementary techniques for probing terahertz magnetic excitations in $Cu_3Bi(SeO_3)_2O_2Cl$. In Proceedings of the International Conference on Infrared, Millimeter, and Terahertz Waves, IRMMW-THz, Wollongong, NSW, Australia, 23–28 September 2012; pp. 1–2.
53. Wang, Z.; Schmidt, M.; Goncharov, Y.; Tsurkan, V.; Krug von Nidda, H.-A.; Loidl, A.; Deisenhofer, J. Terahertz spectroscopy in the pseudo-Kagome system $Cu_3Bi(SeO_3)_2O_2Br$. *Phys. Rev.* **2012**, *B86*, 174411. [CrossRef]
54. Pregelj, M.; Zaharko, O.; Zorko, A.; Gomilšek, M.; Sendetskyi, O.; Günther, A.; Ozerov, M.; Zvyagin, S.A.; Luetkens, H.; Baines, C.; et al. Controllable Broadband Absorption in the Mixed Phase of Metamagnets. *Adv. Funct. Mater.* **2015**, *25*, 3634–3640. [CrossRef]
55. Rousochatzakis, I.; Richter, J.; Zinke, R.; Tsirlin, A.A. Frustration and Dzyaloshinsky-Moriya anisotropy in the kagome francisites $Cu_3Bi(SeO_3)_2O_2X$ (X = Br, Cl). *Phys. Rev.* **2015**, *B91*, 024416. [CrossRef]
56. Zorko, A.; Gomilšek, M.; Pregelj, M.; Ozerov, M.; Zvyagin, S.A.; Ozarowski, A.; Tsurkan, V.; Loidl, A.; Zaharko, O. Electron spin resonance insight into broadband absorption of the $Cu_3Bi(SeO_3)_2O_2Br$ metamagnet. *AIP Adv.* **2016**, *6*, 056210. [CrossRef]
57. Wu, H.C.; Tseng, W.J.; Yang, P.Y.; Chandrasekhar, K.D.; Berger, H.; Yang, H.D. Anisotropic pressure effects on the Kagome $Cu_3Bi(SeO_3)_2O_2Cl$ metamagnet. *J. Phys. D Appl. Phys.* **2017**, *50*, 265002. [CrossRef]
58. Prishchenko, D.A.; Tsirlin, A.A.; Tsurkan, V.; Loidl, A.; Jesche, A.; Mazurenko, V.G. Antiferroelectric instability in the kagome francisites $Cu_3Bi(SeO_3)_2O_2X$ (X = Cl, Br). *Phys. Rev.* **2017**, *B95*, 0264102. [CrossRef]
59. Wu, H.C.; Chandrasekhar, K.D.; Yuan, J.K.; Huang, J.R.; Lin, J.-Y.; Berger, H.; Yang, H.D. Anisotropic spin-flip-induced multiferroic behavior in kagome $Cu_3Bi(SeO_3)_2O_2Cl$. *Phys. Rev.* **2017**, *B95*, 125121. [CrossRef]

60. Gnezdilov, V.; Pashkevich, Y.; Lemmens, P.; Kurnosov, V.; Berdonosov, P.; Dolgikh, V.; Kuznetsova, E.; Pryadun, V.; Zakharov, K.; Vasiliev, A. Lattice and magnetic instabilities in $Cu_3Bi(SeO_3)_2O_2X$ (X = Br, Cl). *Phys. Rev.* **2017**, *B96*, 115144. [CrossRef]
61. Constable, E.; Raymond, S.; Petit, S.; Ressouche, E.; Bourdarot, F.; Debray, J.; Josse, M.; Fabelo, O.; Berger, H.; de Brion, S.; et al. Magnetic and dielectric order in the kagome-like francisite $Cu_3Bi(SeO_3)_2O_2Cl$. *Phys. Rev.* **2017**, *B96*, 014413. [CrossRef]
62. Vergasova, L.P.; Semenova, T.F.; Shuvalov, R.R.; Filatov, S.K.; Anan'lyev, V.V. Ilinskite $NaCu_5O_2(SeO_3)_2Cl_3$—A new mineral of volcanic exhalations. *Trans. Russ. Acad. Sci.-Earth Sci. Sect.* **1997**, *353*, 641–644. (In Russian)
63. Badrtdinov, D.I.; Kuznetsova, E.S.; Verchenko, V.Y.; Berdonosov, P.S.; Dolgikh, V.A.; Mazurenko, V.V.; Tsirlin, A.A. Magnetism of coupled spin tetrahedra in ilinskite-type $KCu_5O_2(SeO_3)_2Cl_3$. *Sci. Rep.* **2018**, *8*, 2379. [CrossRef] [PubMed]
64. Charkin, D.O.; Kayukov, R.A.; Zagidullin, K.A.; Siidra, O.I. Chemical vapor transport and solid-state exchange synthesis of new copper selenite bromides. *Solid State Sci.* **2017**, *64*, 109–113. [CrossRef]
65. Kovrugin, V.M.; Colmont, M.; Mentré, O.; Siidra, O.I. Dimers of oxocentred $[OCu_4]^{6+}$ tetrahedra in two novel copper selenite chlorides, $K[Cu_3O](SeO_3)_2Cl$ and $Na_2[Cu_7O_2](SeO_3)_4Cl_4$, and related minerals and inorganic compounds. *Miner. Mag.* **2016**, *80*, 227–238. [CrossRef]
66. Becker, R.; Berger, H.; Johnsson, M. Monoclinic $Cu_3(SeO_3)_2Cl_2$: An oxohalide with an unusual CuO_4Cl trigonal–bipyramidal coordination. *Acta Cryst.* **2007**, *C63*, i4–i6. [CrossRef]
67. Krivovichev, S.V.; Shuvalov, R.R.; Semenova, T.F.; Filatov, S.K. Crystal chemistry of inorganic compounds based on chains of oxocentered tetrahedral III. Crystal structure of georgbokiite, $Cu_5O_2(SeO_3)_2Cl_2$. *Z. Kristallogr.* **1999**, *214*, 135–138. [CrossRef]
68. Galy, J.; Bonnet, J.J.; Andersson, S. The Crystal Structure of a New Oxide Chloride of Copper (II) and Selenium (IV): $Cu_5Se_2O_8Cl_2$. *Acta Chem. Scand.* **1979**, *A33*, 383–389. [CrossRef]
69. Krivovichev, S.V.; Filatov, S.K.; Burns, P.C.; Vergasova, L.P. The crystal structure of parageorgbokiite, β-$Cu_5O_2(SeO_3)_2Cl_2$. *Can. Miner.* **2007**, *45*, 929–934. [CrossRef]
70. Vergasova, L.P.; Semenova, T.F.; Krivovichev, S.V.; Filatov, S.K.; Zolotarev, A.A., Jr.; Ananiev, V.V. Nicksobolevite, $Cu_7(SeO_3)_2O_2Cl_6$, a new complex copper oxoselenite chloride from Tolbachik fumaroles, Kamchatka peninsula, Russia. *Eur. J. Mineral.* **2014**, *26*, 439–449. [CrossRef]
71. Krivovichev, S.V.; Filatov, S.K.; Semenova, T.F.; Rozhdestvenskaya, L.V. Crystal chemistry of inorganic compounds based on chains of oxocentered tetrahedral, I. Crystal structure of chloromenite, $Cu_9O_2(SeO_3)_4Cl_6$. *Z. Kristallogr.* **1998**, *213*, 645–649. [CrossRef]
72. Vergasova, L.; Krivovichev, S.; Semenova, T.; Filatov, S.; Ananiev, V. Chloromenite, $Cu_9O_2(SeO_3)_4Cl_6$, a new mineral from the Tolbachik volcano, Kamchatka, Russia. *Eur. J. Mineral.* **1999**, *11*, 119–123. [CrossRef]
73. Bastide, B.; Millet, P.; Johnsson, M.; Galy, J. Synthesis of copper(II) and selenium(IV) oxochlorides by chemical transport reaction: Crystal structure of $Cu_9O_2(SeO_3)_4Cl_6$. *Mater. Res. Bull.* **2000**, *35*, 847–855. [CrossRef]
74. Krivovichev, S.V.; Filatov, S.K.; Armbruster, T.; Pankratova, O.Y. Crystal Structure of $Cu(I)Cu(II)_4O(SeO_3)Cl_5$, a New Heterovalent Copper Compound. *Dokl. Chem.* **2004**, *399*, 226–228. [CrossRef]
75. Rabbani, F.; Svengren, H.; Zimmermann, I.; Hu, S.; Laine, T.; Hao, W.; Åkermark, B.; Åkermark, T.; Johnsson, M. Cobalt selenium oxohalides: Catalysts for water oxidation. *Dalton Trans.* **2014**, *43*, 3984–3989. [CrossRef] [PubMed]
76. Johnston, M.G.; Harrison, W.T.A. Barium cobalt chloride selenite, $Ba_2CoCl_2(SeO_3)_2$. *Acta Cryst.* **2002**, *E58*, i49–i51. [CrossRef]
77. Hu, S.; Johnsson, M. Synthesis and crystal structure of $Fe_6Ca_2(SeO_3)_9Cl_4$—A porous oxohalide. *Dalton Trans.* **2013**, *42*, 7859–7862. [CrossRef] [PubMed]
78. Hamida, M.B.; Wickleder, M.S. $\{[CoCl_{2/2}O_{4/1}]\}$-Dimere in der Kristallstruktur von $CoNd_{10}(SeO_3)_{12}Cl_8$. *Z. Kristallogr.* **2005**, *S22*, 141b.
79. Wickleder, M.S.; Hamida, M.B. $CoSm(SeO_3)_2Cl$, $CuGd(SeO_3)_2Cl$, $MnSm(SeO_3)_2Cl$, $CuGd_2(SeO_3)_4$ und $CuSm_2(SeO_3)_4$: Übergangsmetallhaltige Selenite von Samarium und Gadolinum. *Z. Anorg. Allg. Chem.* **2003**, *629*, 556–562. [CrossRef]
80. Krivovichev, S.V.; Filatov, S.K.; Burns, P.C.; Vergasova, L.P. The Crystal Structure of Allochalcoselite, $Cu^+Cu^{2+}{}_5PbO_2(SeO_3)_2Cl_5$, A Mineral With Well-Defined Cu^+ And Cu^{2+} Positions. *Can. Miner.* **2006**, *44*, 507–514. [CrossRef]

81. Burns, P.C.; Krivovichev, S.V.; Filatov, S.K. New Cu^{2+} coordination polyhedra in the crystal structure of burnsite, $KCdCu_7O_2(SeO_3)_2Cl_9$. *Can. Miner.* **2002**, *40*, 1587–1595. [CrossRef]
82. Shuvalov, R.R.; Vegasova, L.P.; Semenova, T.F.; Filatov, S.K.; Krivovichev, S.V.; Siidra, O.I.; Rudashevsky, N.S. Prewittite, $KPb_{1.5}Cu_6Zn(SeO_3)_2O_2Cl_{10}$, a new mineral from Tolbachik fumaroles, Kamchatka peninsula, Russia: Description and crystal structure. *Am. Miner.* **2013**, *98*, 463–469. [CrossRef]
83. Kovrugin, V.M.; Siidra, O.I.; Mentré, O.; Krivovichev, S.V. Structural variety of novel Pb and Bi selenites. *Acta Cryst.* **2013**, *A69*, s134. [CrossRef]
84. Kovrugin, V.M. Crystal Chemistry of Novel Oxide Compounds of Se4+ and Se6+ PhD Thesis Saint Petersburg 2015. Available online: https://disser.spbu.ru/files/phdspsu2015/Kovrugin.pdf (accessed on 3 April 2018).
85. Kovrugin, V.M.; Colmont, M.; Siidra, O.I.; Mentré, O.; Al-Shuray, A.; Gurzhiy, V.V.; Krivovichev, S.V. Oxocentered Cu (ii) lead selenite honeycomb lattices hosting Cu (i) Cl 2 groups obtained by chemical vapor transport reactions. *Chem. Commun.* **2015**, *51*, 9563–9566. [CrossRef] [PubMed]
86. Cao, X.-L.; Kong, F.; Hu, C.-L.; Xu, X.; Mao, J.-G. $Pb_4V_6O_{16}(SeO_3)_3(H_2O)$, $Pb_2VO_2(SeO_3)_2Cl$, and $PbVO_2(SeO_3)F$: New Lead(II)−Vanadium(V) Mixed-Metal Selenites Featuring Novel Anionic Skeletons. *Inorg. Chem.* **2014**, *53*, 8816–8824. [CrossRef] [PubMed]
87. Gemmi, M.; Campostrini, I.; Demartin, F.; Gorelik, T.E.; Gramaccioli, C.M. Structure of the new mineral sarrabusite, $Pb_5CuCl_4(SeO_3)_4$, solved by manual electrondiffraction tomography. *Acta Cryst.* **2012**, *B68*, 15–23. [CrossRef] [PubMed]
88. Vergasova, L.P.; Semenova, T.F.; Filatov, S.K.; Krivovichev, S.V.; Shuvalov, R.R.; Ananiev, V.V. Georgbokiite $Cu_5O_2(SeO_3)_2Cl_2$—A new mineral from volcanic sublimates. In *Doklady Earth Sciences*; Springer: Berlin/Heidelberg, Germany, 1999; Volume 364, pp. 527–531. (In Russian)
89. Semenova, T.F.; Rozhdestvenskaya, I.V.; Filatov, S.K.; Vergasova, L.P. Crystal Structure and Physical Properties of Sophiite, $Zn_2(SeO_3)Cl_2$, a New Mineral. *Miner. Mag.* **1992**, *56*, 241–245. [CrossRef]
90. Johnsson, M.; Törnroos, K.W. Zinc selenium oxochloride, b-$Zn_2(SeO_3)Cl_2$, a synthetic polymorph of the mineral sophiite. *Acta Cryst.* **2007**, *C63*, i34–i36. [CrossRef]
91. Akhrorov, A.Y.; Kuznetsova, E.S.; Aksenov, S.M.; Berdonosov, P.S.; Kuznetsov, A.N.; Dolgikh, V.A. Synthesis and crystal structure of $Fe[(Te_{1.5}Se_{0.5})O_5]Cl$, the first iron compound with selenate(IV) and tellurate(IV) groups. *Solid State Sci.* **2017**, *74*, 37–43. [CrossRef]
92. Pregelj, M.; Zaharko, O.; Zorko, A.; Kutnjak, Z.; Jeglič, P.; Brown, P.J.; Jagodič, M.; Jagličić, Z.; Berger, H.; Arčon, D. Spin Amplitude Modulation Driven Magnetoelectric Coupling in the New Multiferroic $FeTe_2O_5Br$. *Phys. Rev. Lett.* **2009**, *103*, 147202. [CrossRef] [PubMed]
93. Pregelj, M.; Zorko, A.; Zaharko, O.; Arčon, D.; Komelj, M.; Hillier, A.D.; Berger, H. Persistent Spin Dynamics Intrinsic to Amplitude-Modulated Long-Range Magnetic Order. *Phys. Rev. Lett.* **2012**, *109*, 227202. [CrossRef] [PubMed]
94. Zaharko, O.; Pregelj, M.; Arčon, D.; Brown, P.J.; Chernyshov, D.; Stuhr, U.; Berger, H. $FeTe_2O_5Br$ system: New ferroelectric with an incommensurate spin modulation. *J. Phys. Conf. Ser.* **2010**, *211*, 012002. [CrossRef]
95. Choi, K.-Y.; Choi, I.H.; Lemmens, P.; van Tol, J.; Berger, H. Magnetic, structural, and electronic properties of the multiferroic compound $FeTe_2O_5Br$ with geometrical frustration. *J. Phys. Condens. Matter* **2014**, *26*, 086001. [CrossRef] [PubMed]
96. Lafront, A.-M.; Bonvoisin, J.; Trombe, J.-C. Synthesis, Crystal Structure, and Magnetic Measurement of Two New Diselenites:$M_2(Se_2O_5)_3$ with M = Fe(III), Cr(III). *J. Solid State Chem.* **1996**, *122*, 130–138. [CrossRef]
97. Wildner, M. Crystal Structure of $Mn(II)Mn(III)_2O(SeO_3)_3$. *J. Solid State Chem.* **1994**, *113*, 252–256. [CrossRef]
98. Berdonosov, P.S.; Olenev, A.V.; Dolgikh, V.A. Lead (II) selenite halides $Pb_3(SeO_3)_2X_2$ (X = Br, I): Synthesis and crystal structure. *Crystallogr. Rep.* **2012**, *57*, 200–204. [CrossRef]